



MOLECULAR DYNAMICS INVESTIGATION OF MOIRE PATTERNS IN  
DOUBLE-LAYER GRAPHENE

A THESIS SUBMITTED TO  
THE GRADUATE SCHOOL OF NATURAL AND APPLIED SCIENCES  
OF  
MIDDLE EAST TECHNICAL UNIVERSITY

BY

GÖKÇE SÖKMEN

IN PARTIAL FULFILLMENT OF THE REQUIREMENTS  
FOR  
THE DEGREE OF MASTER OF SCIENCE  
IN  
MICRO AND NANOTECHNOLOGY

AUGUST 2012

Approval of the thesis:

**MOLECULAR DYNAMICS INVESTIGATION OF MOIRE PATTERNS IN  
DOUBLE-LAYER GRAPHENE**

submitted by **GÖKÇE SÖKMEN** in partial fulfillment of the requirements for the degree of  
**Master of Science in Micro and Nanotechnology Department, Middle East Technical  
University** by,

Prof. Dr. Canan Özgen  
Dean, Graduate School of **Natural and Applied Sciences**

\_\_\_\_\_

Prof. Dr. Mürvet Volkan  
Head of Department, **Micro and Nanotechnology**

\_\_\_\_\_

Assist.Prof. Dr. Hande Toffoli  
Supervisor, **Physics Department, METU**

\_\_\_\_\_

Assist. Prof. Dr. Daniele Toffoli  
Co-supervisor, **Chemistry Department, METU**

\_\_\_\_\_

**Examining Committee Members:**

Prof. Dr. Şakir Erkoç  
Department of Physics, METU

\_\_\_\_\_

Assist. Prof. Dr. Hande Toffoli  
Department of Physics, METU

\_\_\_\_\_

Prof. Dr. Oguz Gülseren  
Department of Physics, Bilkent Univ.

\_\_\_\_\_

Assist. Prof. Dr. Demirkan Çöker  
Department of Aerospace Engineering, METU

\_\_\_\_\_

Assist. Prof. Dr. Eren Kalay  
Department of Metallurgical and Materials Engineering, METU

\_\_\_\_\_

**Date:**

\_\_\_\_\_

**I hereby declare that all information in this document has been obtained and presented in accordance with academic rules and ethical conduct. I also declare that, as required by these rules and conduct, I have fully cited and referenced all material and results that are not original to this work.**

Name, Last Name: GÖKÇE SÖKMEN

Signature :

# ABSTRACT

## MOLECULAR DYNAMICS INVESTIGATION OF MOIRE PATTERNS IN DOUBLE-LAYER GRAPHENE

Sökmen, Gökçe

M.S., Department of Micro and Nanotechnology

Supervisor : Assist.Prof. Dr. Hande Toffoli

Co-Supervisor : Assist. Prof. Dr. Daniele Toffoli

August 2012, 59 pages

Before Moire patterns are discovered in graphene, graphene was assumed to be found in only the rhombohedral form in nature. After transfer of graphene layer over another substrate was achieved by Andre Geim and Konstantin Novoselov, studies on graphene gained momentum. Following this, moire patterns were observed by scanning tunnelling microscopy (STM) and high resolution transmission electron microscopy (HR-TEM). However, stability of these structures are still unknown. In this thesis, for the first time in literature, molecular dynamics of double layer graphene based Moire patterns are investigated as a result of the rotation of two graphene layers with LAMMPS (Large-scale Atomic/Molecular Massively Parallel Simulator) which has a GNU general public license. To model the two graphene layers, hexagonal graphene layers are generated by home written Octave code. Then, periodicity condition for the Moire patterns are derived in chapter 2 according to rotation of graphene layers around their central axis, perpendicular to the layers. Then these layers with different angles or temperature or size are simulated by LAMMPS.

There are 4 kind of molecular dynamics simulations studied according to modeled flakes.

These are grouped under the name of '*Experiment #*' according to the modeling structure. Experiment-1 simulates double layer hexagonal flakes of graphene at a temperature of 0.1K. Experiment-2 simulates periodic moire patterns under periodic boundary conditions and represents the infinitely large graphene layers at 10K. Experiment 3 is different version of the experiment 1 but at higher temperature (10K). Finally, experiment 4 is modeled to show the behaviour of the graphene flake on a growth or attached region. The atoms around the flakes are modeled as a rigid body and constructs some stress on the graphene flakes.

Keywords: Molecular Dynamics, Graphene, Moire pattern

# ÖZ

## ÇİFT KATMANLI GRAFENDE MOIRE DESENLERİNİN MOLEKÜLER DİNAMİK YÖNTEMİYLE İNCELENMESİ

Sökmen, Gökçe

Yüksek Lisans, Mikro ve Nanoteknoloji

Tez Yöneticisi : Yrd.Doç. Dr. Hande Toffoli

Ortak Tez Yöneticisi : Yrd.Doç. Dr. Daniele Toffoli

Ağustos 2012, 59 sayfa

Grafendeki Moire desenlerinin keşfinden önce grafenin doğada sadece rombohedral biçimde var olduğu sanılırdı. Andre Geim ve Konstantin Novoselov'un grafenin büyütülüp başka bir yüzeye transfer edilebileceğini kanıtlamaları üzerine grafen konusundaki çalışmalar arttı. Sonra yüzey tünelleme mikroskopları ve yüksek çözünürlüklü transmisyon elektron mikroskobu sayesinde moire desenleri gözlemlendi. Ancak bu moire desenlerinin oluşturulduğu yapıların kararlılığı çok bilinen bir şey değil. Bu sebeple bu tezde, literatürde ilk defa grafenin oluşturduğu moire desenlerinin kararlılığı ücretsiz lisansa sahip olan LAMMPS programı kullanılarak moleküler dinamik simülasyonu ile incelendi.

Altıgen grafen yüzeyler, çift katlı grafeni modellemek için inşa edildi. Daha sonra Moire desenlerinin periyodik olma koşulları bölüm 2de türetildi. Daha sonra farklı boyutlarda, açılarda ya da sıcaklıkta oluşturulan yüzeyler LAMMPSda canlandırıldı.

Grafen tabakalarının modellenmesine göre 4 çeşit moleküler dinamik simülasyonu yapıldı. Bunlar '#. deney' adı altında adlandırıldı. 1.Deney, sıcaklığın 0.1K olduğu çift katlı grafen tabakasını modellemektedir. 2.Deney periyodik sınır koşulları altında ifade edilen sonsuz

ift katlı grafen yzeyini tanımlamaktadır. 3.Deney, 1.deneyin farklı bir versiyonudur ancak sıcaklık daha yksektir (10K). Son olarak da 4.deney bir yzey zerinde bytlen grafeni temsilen etrafı birbirine gre sabit atomlarla evrilmiř grafeni temsil etmektedir.

Anahtar Kelimeler: Molekler dinamik, Grafen, Moire desenleri

*To My Family*

## ACKNOWLEDGMENTS

First of all I would like to thank my thesis advisor Assist.Prof.Dr. Hande Toffoli for her help, guidance and support during my graduate studies. Studying of molecular dynamics with her is invaluable for me. I should not forget to thank Prof. Dr. Oğuz Gülseren for his special guidance and friendly attitude during my studies about molecular dynamics. Without his guidance and help, this study could not exist. Special thanks to Assist.Prof.Dr. Danielle Toffoli for providing a room to study and to my brother Buğra Sökmen for accepting me to live with him during my master of science. Moreover, I would like to thank my friends Ceren Canbazoğlu for her psychological support and Alperen Toprak for invaluable contributions to my life. I would also express my gratitude to Dr. Yekbun Adıgüzel, Dr. Zerrin Işık for their advices about graduate study. Last but not least, my special thanks go to my family for their endless support, love and encouragement throughout my whole life.

# TABLE OF CONTENTS

ABSTRACT . . . . .	iv
ÖZ . . . . .	vi
ACKNOWLEDGMENTS . . . . .	ix
TABLE OF CONTENTS . . . . .	x
LIST OF TABLES . . . . .	xii
LIST OF FIGURES . . . . .	xiii
CHAPTERS	
1 INTRODUCTION TO COMPUTER SIMULATIONS AND MOLECULAR DYNAMICS . . . . .	1
1.1 ALGORITHMS OF MOLECULAR DYNAMICS . . . . .	2
1.1.1 Initialization . . . . .	3
1.1.1.1 Boundary Conditions . . . . .	3
1.1.1.2 Force Calculation . . . . .	5
1.1.1.3 Time Step Scaling . . . . .	7
1.1.2 Integrating the Equation Of Motion . . . . .	7
1.1.2.1 Verlet's Algorithm . . . . .	8
1.1.2.2 Predictor-Corrector Algorithm . . . . .	8
1.1.2.3 Comparison Between the Verlet Methods & Predictor-Corrector Methods: . . . . .	10
1.2 THERMODYNAMICS . . . . .	10
1.2.1 Micro Canonical Ensemble . . . . .	11
1.2.2 Canonical Ensemble . . . . .	11
1.3 MOLECULAR DYNAMICS AT CONSTANT TEMPERATURE . . . . .	11
1.3.1 Velocity Scaling . . . . .	12
1.3.2 Berendsen Thermostat . . . . .	12

1.3.3	Langevin Thermostat . . . . .	13
1.3.4	Dissipative Particle Dynamics Thermostat . . . . .	13
1.3.5	Andersen Thermostat . . . . .	14
1.3.6	Nose-Hoover Thermostat . . . . .	15
2	GRAPHENE AND MOIRE PATTERNS . . . . .	16
2.1	GRAPHENE LAYERS . . . . .	20
2.2	MOIRE PATTERN . . . . .	23
2.2.1	Geometric Investigation of Hexagonal Moire Patterns . . . . .	24
3	MOLECULAR DYNAMICS SIMULATION OF GRAPHENE . . . . .	31
3.1	EXPERIMENT 1: Hexagonal graphene . . . . .	33
3.1.1	Graphene Flake With 1448 Atom at 0.1K . . . . .	35
3.1.2	Graphene Flake With 2024 Atoms at 0K . . . . .	40
3.1.3	Graphene Flake With 3884 Atoms at 0K . . . . .	40
3.1.4	Graphene Flake With 5288 Atoms at 0K . . . . .	42
3.2	EXPERIMENT 2: Periodic Moire Layers . . . . .	42
3.3	EXPERIMENT 3: Relaxed Graphene Identified According to Layers . . . . .	46
3.3.1	Graphene Flake With 428 Atoms at 10K . . . . .	46
3.4	EXPERIMENT 4: Stretched Graphene . . . . .	50
4	CONCLUSION . . . . .	53
	REFERENCES . . . . .	56

## LIST OF TABLES

### TABLES

Table 1.1	Gear corrector coefficients . . . . .	10
Table 2.1	Angles for periodic moire pattern for largest unit cells. # of atoms belong to hexagonal double layers. . . . .	27
Table 3.1	Summary of the results of experiment-1. . . . .	35
Table 3.2	Experiment1 with 1448 Atoms at 0K . . . . .	36

# LIST OF FIGURES

## FIGURES

Figure 1.1 Periodicity of simulation box . . . . .	4
Figure 1.2 Lennard Jones Potential graph for Ar . . . . .	5
Figure 2.1 The energy difference between first and last energy levels at the K points for N graphene layers. From ref[31] . . . . .	17
Figure 2.2 Unit cell of graphene . . . . .	18
Figure 2.3 Energy band dispersion and Brillouin zone of graphene . . . . .	19
Figure 2.4 <b>a)</b> Bernal Stacking <b>b)</b> Rhombohedral Stacking (A is grey first layer; B is green second; C is light grey third layer) . . . . .	20
Figure 2.5 Bias voltage vs. measured resistance graphs at different top gate voltages and band diagrams of (a, b) ABC, and (c, d) ABA trilayers. The ABC and ABA trilayers are separated from the top gate by 90 nm and 15 nm dielectric layers, respectively. The bias voltages are applied from the back gate. The solid and the dashed lines in the energy band diagrams represent the cases with and without an external electric field, respectively. A perpendicular external electrical field results in an energy gap in the ABC trilayer and a band overlap in the ABA trilayer [34]. .	22
Figure 2.6 Some moire patterns observed by HRTEM from reference [47]. . . . .	24
Figure 2.7 Graphene flake is constructed as hexagonal layer represented by N for each shell . . . . .	25
Figure 2.8 To identify periodic moire patterns symmetric points according to the sym- metry lines should coincide . . . . .	26
Figure 2.9 Periodic moire pattern is constructed when the atoms are eclipsed at N=6 with $\alpha = 10.4174$ . . . . .	28

Figure 3.1	a)Two graphene layers with 0 degrees with respect to each other. Central atom and neighbor atom on one layer is showed. b) Vectors from central atom to neighbor atom on both layer. The angle between the projections of these vectors to plane, which is perpendicular to the axis passed through central atoms is 0 degree.	32
Figure 3.2	Part of Octave code for calculation of angle.	33
Figure 3.3	The image at the left side shows the initial moire pattern constructed with a 2-degree twist of graphene flakes. The image at the right side shows the same flake after 1.96 nanoseconds. The simulation is performed at approximately 0 K, and the final rotation angle is 4.29 degrees.	37
Figure 3.4	The change in the potential energy and the moire angle with time, which includes 1448 atoms (1332 of them are carbon) and has an initial twisting angle of 2 degrees but initial values did not taken into graph. The final angle stabilizes around 4.29 degrees.	37
Figure 3.5	The change in the potential energy (blue)and kinetic energy (green) with sampling frequency of $10^{13}$ Hz for graphene layer with 1448 atoms initial and final twisting angles are 2 and 4.29 respectively.	38
Figure 3.6	The image at the left side shows the initial moire pattern constructed with a 10-degree twist of graphene flakes. The image at the right side shows the same flake after 0.97 nanoseconds. The simulation is performed at approximately 0 K, and the final twist amount is 4.29 degrees.	38
Figure 3.7	The change in the potential energy and the moire angle with time in simulation 1, which includes 1448 atoms (1332 of them are carbon) and has an initial twisting angle of 10 degrees. The final angle stabilizes around 4.29 degrees.	39
Figure 3.8	The change in the potential energy and the moire angle with time in simulation 3, which includes 1448 atoms (1332 of them are carbon) and has an initial twisting angle of 15 degrees. The final angle again stabilizes around 4.29 degrees.	39
Figure 3.9	The change in the potential energy and the moire angle with time, as obtained for a 2024-atom setup with an initial twisting angle of 20 degrees (initial value not included). The twisting angle stabilizes around 3.62 degrees.	40

Figure 3.10 The change in the potential energy and the moire angle with time, as obtained for a setup with 3884 atoms and an initial twisting angle of 10 degrees. The final angle becomes 2.59 degrees in this case. . . . .	41
Figure 3.11 Metastable states for the flake with 3884 atoms. The image at the left side shows the angle of 5 degrees. The image at the right side shows the same flake at angle of 2.6 degrees. . . . .	41
Figure 3.12 The change in the potential energy and moire angle with time, as obtained from last simulation of experiment 1 where the graphene flake has 5288 atoms with an initial twisting angle of 5 degrees. This simulation is performed at around 0K. . . . .	42
Figure 3.13 Total energy (higher) and potential energy (lower) per atom at 300K . . . .	43
Figure 3.14 Total energy (higher) and potential energy (lower) per atom at 9K . . . .	44
Figure 3.15 The image at the left side shows the moire pattern at 313 ps, and the image at the right side shows the moire pattern at 328 ps. Periodic graphene double layer includes 1016 atoms and a 13.17-degree twisting angle. The pattern moves in the direction of chiral path at 300K. . . . .	45
Figure 3.16 Total energy (higher) and potential energy (lower) per atom at 300K for the periodic system which has 1016 atom and twisting angle of 13.17 degrees . . . .	45
Figure 3.17 Graphene flake has 428 atoms at around 10K. Diffent twisting initial angles begin from 6 degrees to 14 degrees stabilize at around 8.5 degrees along 2,200,000 timestep. . . . .	47
Figure 3.18 Graphene flake has 428 atoms at around 10K. Various initial twisting angles started from 15 to 23 degrees are shown. Initial angles starts from 21,22,23 degrees falls down to aproximately 7 degrees. . . . .	47
Figure 3.19 Graphene flake has 428 atoms at around 10K. Initial twisting angles started from to 42 degrees to 51 degrees takes the approximate value of 47.7 degrees. . .	48
Figure 3.20 Graphene flake has 428 atoms at around 10K. Initial twisting angles started from to 52 degrees to 60 degrees take average final value of 60 degrees. . . . .	48
Figure 3.21 Graphene flake has 428 atoms at around 10K. Initial twisting angles started from to 6 degrees to 60 degrees and corresponding final angles are shown. Final angles of 60, 47.7 and 8.5 shows most stable conditions. . . . .	49

Figure 3.22 The images of graphene flakes with 428A. . . . .	50
Figure 3.23 Perspective view of graphene flake which has 428 atoms at around 10K at the timestep of 821.000. Some bonds near edge are broken because of stress. Initial angle is given as 5 degrees . . . . .	51
Figure 3.24 Initial and final view of graphene flake which has 428 atoms at around 10K. Some bonds near edge are broken because of stress. Initial angle is given as 5 degrees . . . . .	52
Figure 3.25 Average potential energy at with given initial theta of graphene flakes which has 428 atoms at 10K. Potential wells are seen between maximum points. First maximum occurs at 8 degrees with the potential energy 2822.01 eV; Second maximum occurs at 15 degrees with 2822.99 eV; Third maximum occurs at 30 degrees with 2823.22 eV; Forth maximum occurs at 33 degrees with the potential energy of 2823.16eV; Fifth maximum is at 48 degrees with 2822.88 eV and last maximum is at 55 degrees with 2821.77 eV. . . . .	52

# CHAPTER 1

## INTRODUCTION TO COMPUTER SIMULATIONS AND MOLECULAR DYNAMICS

Computer simulations are handy tools in the sense that they enable predicting the outcomes of various scientific experiments without spending the effort and time that is required to actually construct them. The success of a simulation strongly depends on the correct modeling of all the involved materials, devices, and structures. However, it should be noted that the accurate modeling of a structure may depend on the spatial scale, such as the necessity of considering the quantum effects in nano-scales. In order to overcome this problem, multi-scale modeling techniques have been developed [1]. These techniques prove very useful in today's world, where scientists fabricate new kinds of sensors in nano-scales, in which molecular behaviors are very important. Efficiency of these nano-fabrication techniques also depends on the molecular behavior. Therefore, various molecular-level simulations are used in different areas of nanotechnology [2]. There are two main computational techniques for molecular-level simulations, which are Monte Carlo and molecular dynamics(MD) methods. Monte Carlo molecular simulation method depends on probability distributions in statistical physics. On the other hand, molecular dynamics method uses Newton's equations and solves classical equations of motion at each step. In this latter method, the calculated motion of the ensemble of atoms can be used to extract useful microscopic and macroscopic information such as transport coefficients, phase diagrams, and structural or conformational properties. Of the two main molecular-level simulation techniques mentioned above, molecular dynamics simulations have some advantages over Monte Carlo simulations. These can be listed as follows:

- Calculating the heat capacity, compressibility and interfacial properties can be done

more efficiently using molecular dynamics simulations.

- Dynamic quantities, such as transport coefficients and time correlation functions, cannot be obtained as accurately by Monte Carlo simulations as by molecular dynamics simulations.
- The required time to run a molecular dynamics simulation can be estimated as a multiple of the relaxation time of the studied phenomenon. On the other hand, estimating the duration of a Monte Carlo simulation is more difficult [3]. Monte Carlo transition rules are fine for a system in thermal equilibrium; however, they are not useful for determining the time required to change the microstate or the transition [4].

The molecular dynamics theory was introduced for the first time by Alder and Wainwright in the late 1950s with their model of interaction between hard spheres. In this model, particles are assumed to move at constant velocity with perfectly elastic collisions [5]. Then, Rahman solved the Lennard-Jones model with a step by step approach, where the forces change continuously with changing displacement of particles. In a subsequent work, Verlet time integration algorithm was developed by Verlet [6]. There are several other works developed concerning the computer simulations of molecules, as can be found in many molecular dynamics books [7,8].

## **1.1 ALGORITHMS OF MOLECULAR DYNAMICS**

The main aim of the atomistic simulations are modeling, analyzing, and understanding the motion of the each atom in the material. Molecular dynamics calculates the time dependent behavior of a molecular system by integrating the equations of motion. The fundamental algorithm of molecular dynamics can be described in three steps: (1) Initialization: selecting the initial properties of the system, (2) Equilibration: solving Newton's equations of motion until the system properties converge, and (3) Calculation of the system dynamics: sampling the averages.

### 1.1.1 Initialization

The initial description of a system is very important for the simulation results, which should be comparable with experimental results. In order to be able to work in the classical picture, the type of particles chosen is crucial. Since MD uses Newton's equations instead of Schrodinger's equation, the deBroglie wavelength should be much larger than the interparticle distance. For quantum effects to be insignificant, larger particles, whose deBroglie wavelength is small ( $\lambda = \frac{h}{\sqrt{2mE}}$ ), are preferable. For this reason, MD cannot be applied to smaller particles such as electrons. After determining the types of atoms, initial position and velocities are assigned. An appropriate interaction potential is chosen to derive the forces between the particles. Boundary conditions, thermostat, or barostat is chosen depending on the ensemble. And finally, an optimal time step is set. Here specific properties of these parameters are given in general. The requirements of the graphene system are explained in the last chapter.

#### 1.1.1.1 Boundary Conditions

Molecular dynamics simulation takes place in a simulation box. The size of this simulation box is determined by boundary conditions. The most commonly used boundary condition is the periodic boundary condition since it can represent an infinite number of atoms by performing the simulation in only a single unit cell. Fixed or free boundary conditions are among the other possibilities.

#### Periodic Boundary Condition

The edge effects due to actual physical walls can be eliminated by applying periodic boundary conditions. Particles inside the main simulation box are copied to other boxes. If any particle moves out of the box from one edge, then it enters to the box from the opposite edge. This is provided in the following way: Let us assume that the size of the simulation box in x direction is L, beginning from  $-L/2$  and ending at  $L/2$ . If the new x position of particle is greater than  $L/2$ , then, the new coordinate is adjusted to be  $x-L$ . Similarly, if the new position is less than  $-L/2$ , then, it is replaced by  $x+L$ . Consequently, the problem of the missing of the atoms is prevented. Interaction distance is determined by the cut-off distance of the used potential

function, which will be explained subsequently. For instance, according to Figure 1.1, the particle 3 is in interaction with particles 1, 2, 4, and 6 as determined by the cut-off distance. It should be noted that the distance between the particles 3 and 6 is larger than the cut-off distance when only a single unit cell is considered; however, the actual distance is smaller due to the periodicity as shown in the figure.

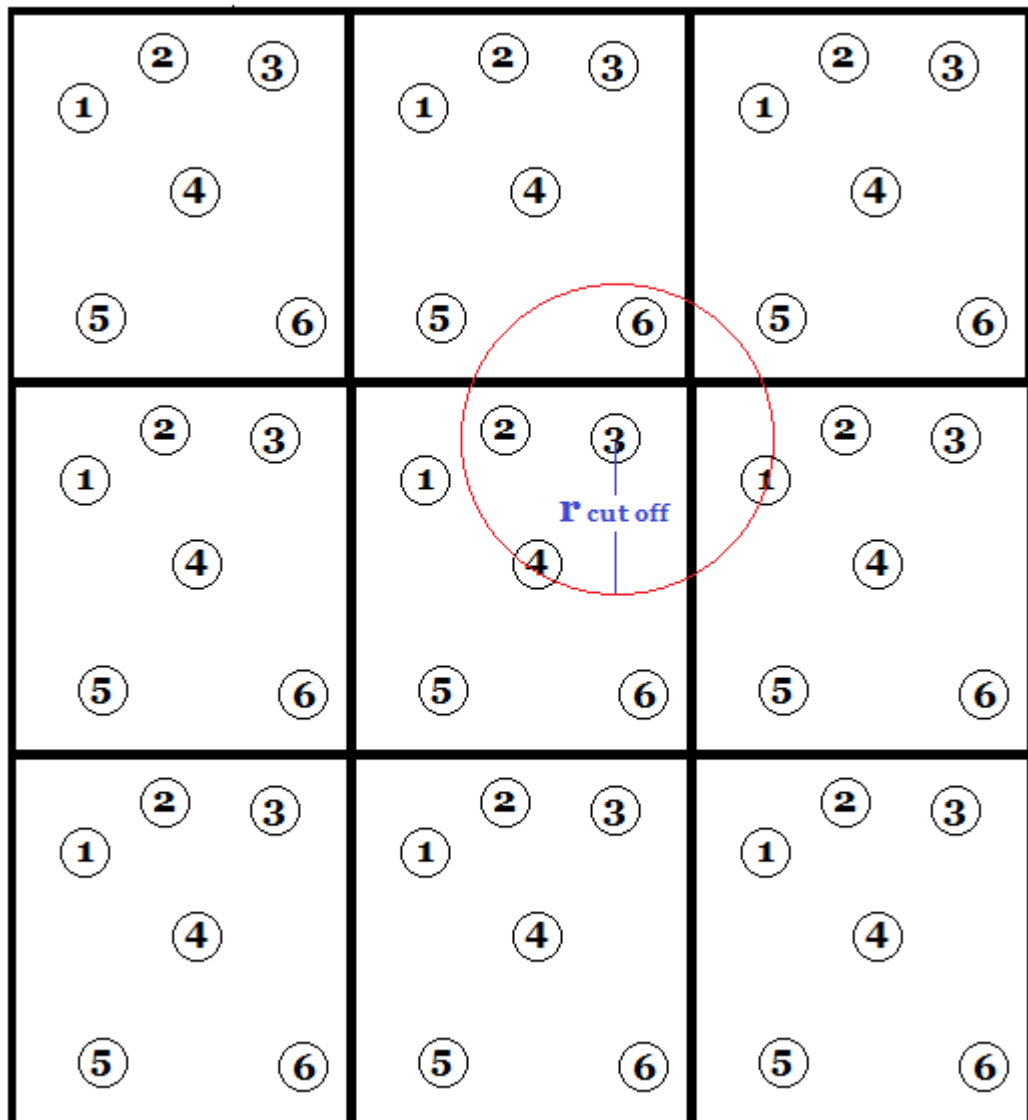


Figure 1.1: Periodicity of simulation box

## Fixed Boundary Condition

Fixed boundary conditions are used when the boundary effects are important. Interaction of the particles with the wall in a liquid simulation in a microchannel [9], grain boundary or dislocation effects in a nano-scale material can be modeled by fixed boundary conditions [10].

### 1.1.1.2 Force Calculation

The forces between the atoms and molecules can be obtained from two- body and many-body interatomic molecular potentials [12]. If the potential function on the  $i$ th atom in the  $N$  number of atom is  $U$ , then the force on this  $i$ th atom can be written as:

$$\vec{F} = -\vec{\nabla}U.$$

The Lennard-Jones (LJ) potential is the simplest approximation that is derived for interatomic potential  $U$  of argon atoms by J.E.Jones [13]. It can be generalized as:

$$U_{LJ} = 4\varepsilon\left[\left(\frac{\sigma}{r}\right)^{12} - \left(\frac{\sigma}{r}\right)^6\right] = \varepsilon\left[\left(\frac{r_m}{r}\right)^{12} - 2\left(\frac{r_m}{r}\right)^6\right]$$

where  $(\sigma, -\varepsilon)$  corresponds to the minimum point of the potential function. Physically  $\sigma$  is the bond distance and  $-\varepsilon$  is the dimer binding energy. The graph of the LJ potential with the values  $\sigma = 3.405\text{\AA}$  and  $-\varepsilon = 119.2\text{K}$  for Ar is given in Figure 1.2.

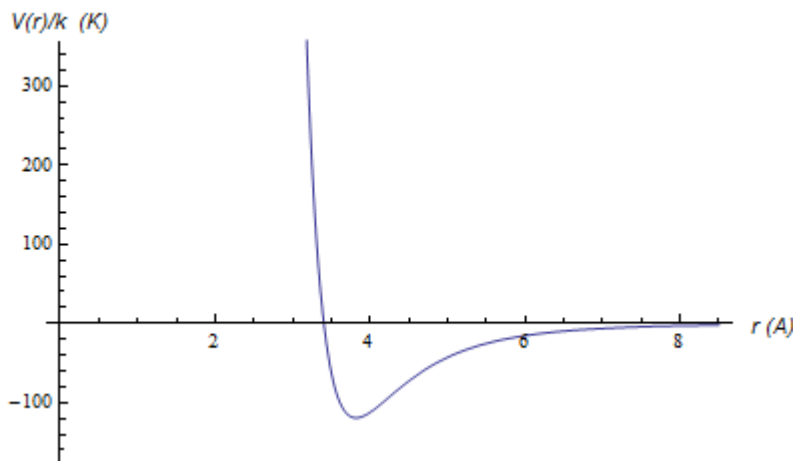


Figure 1.2: Lennard Jones Potential graph for Ar

Calculation of the potential  $U$  for other systems is a more complex process.  $U$  is in general, a

function of interatomic distances and bond angles, and contains various adjustable parameters. While the LJ potential works rather well for noble gases it is usually referred to as an empirical potential since it usually involves obtaining experimental force-distance measurements by surface probe microscopy or microelectrophoretic measurements matched to ab initio computer simulations [8]. Intermolecular potentials are developed according to the type of the materials, such as whether they are metallic, semi-metallic, semiconducting, or organic systems. They can include two-body, three-body, or many-body interactions and angular terms. Some of the most common potential functions are listed below, and detailed information can be found in [12]. In the list provided below, interatomic potentials are classified by type of material.

#### **a) Interatomic Potentials For Metallic Systems**

- The Many-Body Embedded-Atom Model (EAM) Potentials
- The Many-Body Finnis and Sinclair (FS) Potentials
- The Many-Body Sutton and Chen (SC) Long-Range Potentials
- The Many-Body Murrell-Mottram (MM) Potential
- The Many-Body Rafii-Tabar and Sutton (RTS) Long-Range Alloy Potentials
- Angular-Dependent Potentials

#### **b) Interatomic Potentials for Covalently-Bonding Systems**

- The Tersoff Many-Body C-C, Si-Si and C-Si Potentials
- The Brenner-Tersoff-Type First Generation Hydrocarbon Potentials
- The Brenner-Tersoff-Type Second Generation Hydrocarbon Potentials

#### **c) Interatomic Potentials for Non-Covalent Systems**

- The Lennard-Jones and Kihara Potentials
- The exp-6 Potential

- The Ruoff-Hickman Potential

#### d) Interatomic Potential for Metal-Carbon System

#### e) Atomic Site Stress Field

##### 1.1.1.3 Time Step Scaling

Time step is constrained by the vibrational motions of the atoms in solids or liquids. This limits the time step to femtosecond scale [15, 14]

##### 1.1.2 Integrating the Equation Of Motion

The laws of motion are described by ordinary differential equations, where the relevant functions, such as position or velocity depends only on time in classical particle dynamics. For a system consisting of  $N$  particles, there are  $3N$  second order differential equations, which are described by the equation:

$$\mathbf{f}_i = m_i \ddot{\mathbf{r}}. \quad (1.1)$$

Alternatively, this system may be described by a set of  $6N$  first order differential equations, described as:

$$\dot{\mathbf{r}} = \frac{\mathbf{p}_i}{m_i}, \quad (1.2)$$

$$\dot{\mathbf{p}}_i = -\nabla V = \mathbf{f}_i. \quad (1.3)$$

With initial values,  $\mathbf{r}(t_0) = \mathbf{r}_0$  and  $\mathbf{p}(t_0) = \mathbf{p}_0$ , the equations can be solved by Runge-Kutta method. First order RK method of algorithm is called Euler's method.

$$x(t + \Delta t) = x(t) + \dot{x}\Delta t. \quad (1.4)$$

The Runge-Kutta method is slow for large number of molecules, therefore, two other algorithms are developed for molecular dynamics simulations: (1) Verlet's algorithm, which uses the velocities and the positions from previously calculated steps, and (2) Predictor-corrector algorithm, which estimates the velocities and the positions of future steps [16].

### 1.1.2.1 Verlet's Algorithm

Verlet's algorithm is derived by the Taylor expansion of the position:

$$x(t + \Delta t) = x(t) + \frac{dx(t)}{dt}\Delta t + \frac{1}{2}\frac{d^2x(t)}{dt^2}(\Delta t)^2 + \frac{1}{3!}\frac{d^3x(t)}{dt^3}(\Delta t)^3 + \frac{1}{4!}\frac{d^4x(t)}{dt^4}(\Delta t)^4 + \dots, \quad (1.5)$$

$$x(t - \Delta t) = x(t) - \frac{dx(t)}{dt}\Delta t + \frac{1}{2}\frac{d^2x(t)}{dt^2}(\Delta t)^2 - \frac{1}{3!}\frac{d^3x(t)}{dt^3}(\Delta t)^3 + \frac{1}{4!}\frac{d^4x(t)}{dt^4}(\Delta t)^4 + \dots \quad (1.6)$$

When the equation (1.5) added to (1.6), the odd-powered terms disappear yielding

$$x(t + \Delta t) = 2x(t) - x(t - \Delta t) + \frac{d^2x(t)}{dt^2}(\Delta t)^2 + \frac{2}{4!}\frac{d^4x(t)}{dt^4}(\Delta t)^4 + \dots \quad (1.7)$$

The Verlet algorithm requires two steps to reach the future position from the present and past position information. An initialization of the algorithm can thus be done by using the initial position and velocity information and applying the Euler method as given in Equation (1.4). The initial velocity distribution is given according to statistical mechanical requirements of the system. Verlet algorithm does not use velocity information afterwards. The velocity at time  $t$  can be calculated using the central difference method, which can be expressed using the equation

$$v(t) \approx \frac{x(t + \Delta t) - x(t - \Delta t)}{2\Delta t}. \quad (1.8)$$

### 1.1.2.2 Predictor-Corrector Algorithm

This method includes 3 parts, named prediction, force evaluation, and correction, and it is named as PEC algorithm, where P stands for prediction, E for evaluation, and C for correction. Evaluation and correction parts can be repeated many times by using corrected positions and velocities as predicted information. The case where the evaluation and correction steps are repeated only one time is shown by the expression  $PEC(EC) = P(EC)^2$ .  $P(EC)^n$  means that the evaluation and correction steps are repeated for  $n$  times. However, this procedure is not efficient for MD simulations since it requires the calculation of the forces, which is a quite time consuming operation. Gear's Predictor-Corrector algorithm, which is firstly used by Rahman in MD simulations, is given below to explain the steps of this algorithm [16].

**1)Prediction:** Future position can be predicted by applying the Euler method or Taylor expansion using the current position information and its time derivative .

$$\mathbf{r}_p(t + \Delta t) = \mathbf{r}(t) + \mathbf{v}(t)\Delta t + \frac{1}{2}\mathbf{a}(t)(\Delta t)^2 + \frac{1}{3!}\mathbf{b}(t)(\Delta t)^3 + \dots, \quad (1.9)$$

$$\mathbf{v}_p(t + \Delta t) = \mathbf{v}(t) + \mathbf{a}(t)\Delta t + \frac{1}{2}\mathbf{b}(t)(\Delta t)^2 + \dots, \quad (1.10)$$

$$\mathbf{a}_p(t + \Delta t) = \mathbf{a}(t) + \mathbf{b}(t)\Delta t + \dots, \quad (1.11)$$

$$\mathbf{b}_p(t + \Delta t) = \mathbf{b}(t) + \dots \quad (1.12)$$

where  $\mathbf{r}_p$ ,  $\mathbf{v}_p$ ,  $\mathbf{a}_p$ , and  $\mathbf{b}_p$  are predicted positions, velocities, and higher order time derivatives of positions  $\mathbf{r}_p$ .

**2)Force Evaluation:** Force is calculated by taking the gradient of the potential function. Then, the acceleration is calculated by

$$\mathbf{a}_i = \mathbf{f}_i/m_i. \quad (1.13)$$

This calculated acceleration will be different from the predicted acceleration that is calculated in the first step. The difference between these values gives error signal.

**3)Correction:**Equations given in the prediction step cannot give the exact trajectories in time since they do not include the equation of motion, and the acceleration is calculated after the force evaluation. The size of the resultant error is estimated at correction step by taking the difference between the corrected and predicted values. The error of acceleration can be written as follows:

$$\Delta\mathbf{a}(t + \Delta t) = \mathbf{a}_C(t + \Delta t) - \mathbf{a}_P(t + \Delta t). \quad (1.14)$$

The corrected values can be then expressed as:

$$\Delta\mathbf{r}_C(t + \Delta t) = \mathbf{r}_P(t + \Delta t) - C_0\Delta\mathbf{a}(t + \Delta t), \quad (1.15)$$

$$\Delta\mathbf{v}_C(t + \Delta t) = \mathbf{v}_P(t + \Delta t) - C_1\Delta\mathbf{a}(t + \Delta t), \quad (1.16)$$

$$\Delta\mathbf{a}_C(t + \Delta t) = \mathbf{a}_P(t + \Delta t) - C_2\Delta\mathbf{a}(t + \Delta t), \quad (1.17)$$

$$\Delta\mathbf{b}_C(t + \Delta t) = \mathbf{b}_P(t + \Delta t) - C_3\Delta\mathbf{a}(t + \Delta t). \quad (1.18)$$

The coefficients  $C_0, C_1, C_2, C_3, \dots$  are called Gear parameters, which are listed in Table 1.1 as presented in [17,18].

Table 1.1: Gear corrector coefficients

Order	$c_0$	$c_1$	$c_2$	$c_3$	$c_4$	$c_5$
3	0	1	1			
4	$\frac{1}{6}$	$\frac{5}{6}$	1	$\frac{1}{3}$		
5	$\frac{19}{120}$	$\frac{3}{4}$	1	$\frac{1}{2}$	$\frac{1}{12}$	
6	$\frac{3}{20}$	$\frac{251}{360}$	1	$\frac{11}{18}$	$\frac{1}{6}$	$\frac{1}{60}$

### 1.1.2.3 Comparison Between the Verlet Methods & Predictor-Corrector Methods:

When the Verlet algorithm is compared to the predictor-corrector algorithm, it is seen that higher order Gear methods are more accurate for short time step,  $\Delta t$ , values. Gear method results in good local energy conservation, which has only small fluctuations compared to the Verlet method. The Gear method can be used with velocity dependent forces unlike the Verlet algorithm: For instance, it is preferred for constant temperature simulations with Nose-Hoover thermostat since the Verlet method can not be used when forces depend on the velocities of the atoms. It is also easy to use with multiple time step algorithms. On the other hand, the main disadvantage of the Gear method is that the energy error increases linearly with time step  $\Delta t$ . Consequently, the Verlet method is preferred for larger  $\Delta t$  because of its long term energy conservation capability although the energy fluctuations are higher for long time simulations. Another advantage of the Verlet method is that it is time reversible while the Gear method is not.

## 1.2 THERMODYNAMICS

An ensemble includes all the possible states of a system. There are many types of ensemble where one parameter is fixed. Generalising ensembles for molecular dynamics is complicated because equation of motion lead to naturally to microcanonical ensemble (NVE). However temperature is the main parameter to discuss about energy of the system in the real experiment. Therefore mainly NVT ensemble is in our case.

### **1.2.1 Micro Canonical Ensemble**

In the micro canonical ensemble, the number of the particles, and the volume and the energy of the system are constant. Therefore, this ensemble is also called an NVE ensemble. Molecular dynamics simulations naturally fit the NVE ensemble because energy is conserved by Newton's equations of motion. Initial velocity can take any random value or assigned to zero. They will be corrected in the integrator phase of the algorithm. Similar to velocity assignment any time derivatives of position except acceleration can be assigned to zero. Initial accelerations are determined from Newton's equation during the simulation.

### **1.2.2 Canonical Ensemble**

In the canonical ensemble, number of particles (N), volume (V), and temperature (T) are fixed. Temperature describes the statistics of a system which is only a parameter in canonical ensemble. Fluctuation in the temperature is required for statistical physics. Both averaging the temperature to fixed value at the same time enabling the fluctuation is provided by thermostats in molecular dynamics simulations.

## **1.3 MOLECULAR DYNAMICS AT CONSTANT TEMPERATURE**

Temperature is a known thermodynamical variable in real experiments unlike the energy of the system, which cannot be measured directly. It must be constant in some situations, such as the study of temperature induced unfolding of proteins, which requires a precise temperature control [19]. The fluctuations in the temperature are small for large NVE systems; therefore, the temperature can be considered as constant for such systems. Consequently, canonical NVT ensemble is used with appropriate temperature control methods. Thermostats are introduced to control the temperature, and they are generally based on the coupling of system with a heat bath, which has an infinite amount of energy at constant temperature. There are mainly 3 ways to control the temperature in a molecular dynamics simulation. These are:

1. Scaling velocities (e.g. simple velocity scaling and the Berendsen thermostat)
2. Adding stochastic forces and/or velocities (e.g., the Andersen, Langevin, and Dissipa-

tive Particle Dynamics thermostats)

### 3. Using extended Lagrangian formalisms (e.g., the Nose-Hoover thermostat)

#### 1.3.1 Velocity Scaling

Desired temperature( $T_f$ ) can be achieved by multiplication of the velocity with a scale factor( $\zeta$ ), which is defined as

$$\zeta = \frac{v_f}{v_i} = \sqrt{\frac{T_f}{T_i}} \quad (1.19)$$

where  $T_i$  and  $v_i$  are the instantaneous values and  $T_f$  and  $v_f$  are the desired values of the temperature and velocity, respectively. If the scaling is done at every step, velocity scaling schemes can not follow the canonical ensemble since this causes all microscopic kinetic energy values to be identical. This technique is used in a controlled way in the NVE ensemble, where the temperature scaling is less important than the energy scaling such as the initialization step [20].

#### 1.3.2 Berendsen Thermostat

This thermostat also tries to correct the deviations of the instantaneous temperature values from the predicted ones by multiplying the velocities by a certain factor. Berendsen introduced a weak coupling to the external heat bath in order to enable temperature fluctuation, which cannot be obtained in the velocity scaling method. The heat bath can provide heat to or absorb heat from the system. The rate of the change in the actual temperature is related to desired temperature, which is equal to the bath temperature, can be expressed as

$$\frac{dT}{dt} = \frac{T_f - T_i}{\tau} \quad (1.20)$$

where  $\tau$  is the coupling parameter and shows the rise time of the temperature. The change in the temperature in a time step can be given by

$$\Delta T = \Delta(t) \frac{T_f - T_i}{\tau}. \quad (1.21)$$

Consequently, the scaling factor becomes

$$\zeta = \frac{v_f}{v_i} = \sqrt{\frac{T_f}{T_i}} = \sqrt{1 + \frac{\Delta T}{T_i}} = \sqrt{1 + \frac{\Delta t}{\tau} \frac{T_f - T_i}{T_i}}. \quad (1.22)$$

In such a system,  $\tau$  determines the characteristics of the ensemble. When it is very large, Berendsen thermostat is inactive and the run samples a microcanonical ensemble. On the other hand, unrealistic low temperature fluctuations are observed when  $\tau$  is too small.  $T_i$  is initial temperature whereas  $T_f$  is desired temperature determined by heat bath.

### 1.3.3 Langevin Thermostat

Atoms in the system are assumed to be surrounded by a sea of smaller sized fictional particles in the Langevin dynamics. Particles in a fluid are represented by Brownian motion and can be an example to the use of the Langevin equation. Therefore, Langevin dynamics can be described by Langevin equation, which has additional stochastic component including random damped velocity additional to the force on the particle and a term depended on white noise which is given as a third term in the equation below [21]:

$$M\ddot{x}(t) = -\nabla U - \gamma M\dot{x}(t) + \sqrt{2k_B T \gamma M} \xi(t) \quad (1.23)$$

where  $U$  is the particle interaction potential,  $M$  is mass of particle,  $\gamma$  is friction coefficient in the units of  $1/time$ , and  $\xi$  is delta-correlated stationary Gaussian distributed random force, satisfying:

$$\langle \xi(t) \rangle = 0, \quad (1.24)$$

$$\langle \xi(t)\xi(t') \rangle = \delta(t - t'). \quad (1.25)$$

With the use of Langevin thermostat, each particle is coupled to a local heat bath [22]. If the system is too hot, particles are slowed down by the friction coefficient, and otherwise, more energy is added to the system by noise term. These two factors are balanced to give a constant temperature. The disadvantage of this thermostat is non-conservation of momentum for collision like processes [22].

### 1.3.4 Dissipative Particle Dynamics Thermostat

Dissipative particle dynamics (DPD) include local friction and noise depended forces. However, the friction does not dampen the absolute velocities of the particle, it dampens the relative velocities between particles. Therefore, this method is more sensitive to velocity gradients in order to be consistent with hydrodynamics. The equation of motion for DPD can be

described in this way:

$$\dot{\vec{r}}_i = \frac{\dot{\vec{p}}_i}{m_i}, \quad (1.26)$$

$$\dot{\vec{p}}_i = \vec{F}_i + \vec{F}_i^D + \vec{F}_i^R \quad (1.27)$$

where D refers to the damping (or dissipative) force  $\vec{F}_i^D$  on particle i, and R refers to random force  $\vec{F}_i^R$ . These forces are the sums of the corresponding forces on the particle pairs:

$$\vec{F}_i^D = \sum_{i \neq j} \vec{F}_{ij}^D, \quad (1.28)$$

$$\vec{F}_i^R = \sum_{i \neq j} \vec{F}_{ij}^R. \quad (1.29)$$

Dissipation force and random force can be described by these equations:

$$\vec{F}_{ij}^D = -\gamma \cdot W^D \cdot (\hat{r}_{ij} \cdot \vec{v}_{ij}) \cdot \hat{r}_{ij} \quad (1.30)$$

$$\vec{F}_{ij}^R = \sqrt{2k_B T \gamma} \cdot W^R \cdot \theta_{ij} \cdot \hat{r}_{ij} \quad (1.31)$$

where  $\vec{v}_{ij} = \vec{v}_i - \vec{v}_j$  is the relative velocity between particles i and j,  $\hat{r}_{ij}$  is the unit vector in the direction of  $\vec{r}_{ij} = \vec{r}_i - \vec{r}_j$ , the distance between particles i and j, and  $\gamma$  is the friction constant.  $W^D$  and  $W^R$  are interatomic distance dependent weight functions vanishing for  $r_{ij} \geq r_c$ , where  $r_c$  is cutoff distance.

$$(W(r)^R)^2 = W^D(r) \quad (1.32)$$

$$(W(r)^R)^2 = W^D(r) = \begin{cases} (1 - r_{ij}/r_c)^2 & , r < r_c \\ 0 & , r \geq r_c \end{cases} \quad (1.33)$$

Dissipative particle dynamics thermostat can be a good choice to study hydrodynamics because of its momentum conservation property; however, it is not suggested for heat flow calculations [22,23].

### 1.3.5 Andersen Thermostat

This thermostat is proposed by Andersen [24]. The system is coupled to a heat bath, which is constructed by stochastic impulsive forces that act periodically on randomly selected particles [25]. Random velocities that fit into the Maxwell distribution of velocity are assigned to randomly selected particles instead of solving the Langevin equation. As a result, a canonical distribution is established, however, the momentum is not conserved. Thermostatting is

not homogenous with respect to neither space nor time. A momentum conserving Andersen thermostat is developed by Lowe [26]. Andersen-Lowe thermostat can be preferred in some situations because of its computational efficiency [22].

### 1.3.6 Nose-Hoover Thermostat

Nose extended the Lagrangian formalism by adding some imaginary variables, and Hoose changed its formalism in more understandable way. What it is done fits also Hamiltonian equations. Therefore, the properties of microcanonical ensemble are conserved. To understand whether it fits the canonical ensemble, someone should look at the partition function which should include Boltzman factor. Extended Langrange equation is written as [27]:

$$L_H = \sum_{i=1}^N \frac{m_i}{2} s^2 \dot{r}_i^2 - U(r^N) + \frac{Q\dot{s}^2}{2} - g_{dof} \cdot k_B \cdot T \cdot \ln s \quad (1.34)$$

$$(1.35)$$

where s is some kind of a scale factor. If real parameters are defined with apostrophe, dependence on virtual parameters can be written in this way:

$$\vec{r}'_i = \vec{r}_i, \quad (1.36)$$

$$\vec{p}'_i = \frac{\vec{p}_i}{s}, \quad (1.37)$$

$$t' = \int_0^t \frac{dt}{s}. \quad (1.38)$$

## CHAPTER 2

### GRAPHENE AND MOIRE PATTERNS

Carbon is the first element of group IV of the periodic table. Isolated Carbon atom has the  $1s^2 2s^2 2p^2$  electronic configuration. Three kind of hybridization occurs in carbon.

**1)  $sp$  hybridization:**  $sp$  hybridization is the case where a 2s orbital overlaps with one 2p orbital. Two of the four valence electrons fill the hybridized orbital and they are called  $sp$  valance electrons. The other two electrons occupy the unhybridized 2p orbitals. Acetylene,  $HC\equiv HC$ , is an example of  $sp$  hybridization. It has triple bond with one  $\sigma$  and two  $\pi$  bonds.

**2)  $sp^2$  hybridization:**  $sp^2$  hybridization is the case where a 2s orbital overlaps with two 2p orbitals. Three of the four valence electrons fill the three hybridized orbitals, and they are called  $sp^2$  valance electrons. The remaining electron occupies the unhybridized 2p orbital.  $2sp^2$  orbitals result in a 120 degree angle between the bonds on the same plane, which is perpendicular to the 2p orbital. Graphene and polyacetylene  $(HC - CH-)_n$  are examples of this kind of hybridization.

**3)  $sp^3$  hybridization:**  $sp^3$  hybridization is the case where the 2s orbital overlaps with three 2p orbitals. Four valence electrons are distributed among these four hybridized orbitals, and they are called  $sp^3$  valance electrons. The angles between each of these orbitals are 109.5 degrees to each other, resulting in a geometric configuration referred as tetrahedral. Diamond and Methane ( $CH_4$ ) are examples of  $sp^3$  hybridization.

Carbon atoms share electron pairs, and consequently, form covalent bonds. Various known carbon allotropes such as diamond, graphite, various types of fullerene, and several kinds of nanotubes are the results of this volatile bonding structure.

**Graphene:** Graphene is an outstanding material in which many researchers have been interested for 65 years. However, it gained popularity after Andre Geim and Konstantin Novoselov won the 2010 Nobel Prize in Physics by showing that it can be fabricated as a stand-alone material. Initial large scale graphene layer fabrication for touch screens was achieved by a roll to roll process for size of 30 inch. This technique requires CVD growth of graphene on a copper foil followed by coating with a polymer, then copper etching, and finally, transferring of the graphene to the target layer [28]. Many useful properties of graphene make it an ideal material for possible future improvements in microelectronics. One example is graphene transistors that are used to measure the action potentials of cardiomyocyte-like HL-1 cells [29]. This study also shows that graphene is a biocompatible material. Consequently, it can be an important material for the development of biochips. Thermal properties of graphene make it a good thermal interface material, which are very important materials used to prevent the overheating of computers [30]. Furthermore, graphene has excellent electronic properties: It is a two dimensional material in terms of electron localization. According to tight-binding method used by B.Partoens and F. M. Peeters, graphene shows three dimensional electronic property of graphite with more than 10 layer of graphene [31]. The energy difference between the valence and the conduction bands difference at the K point for N graphene layers are given in Fig.2.1.

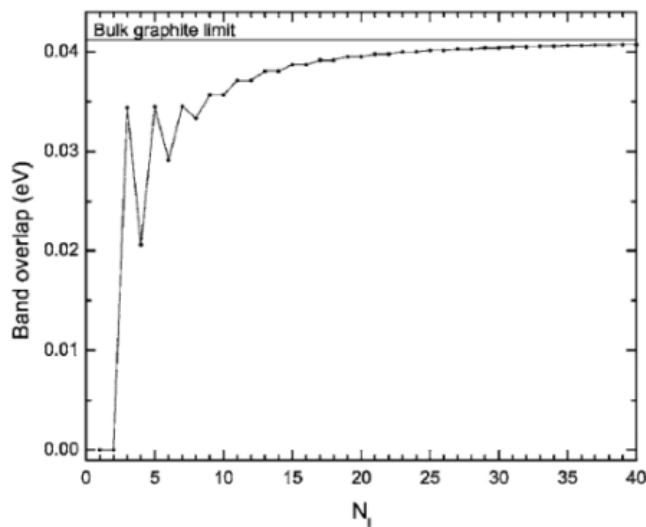


Figure 2.1: The energy difference between first and last energy levels at the K points for N graphene layers. From ref[31]

Carbon atoms are placed in the corners of hexagons in the graphene sheet, which seems like

a honey comb. Each atom is bonded to its three nearest neighbors via  $sp^2$  trigonal, very strong, single  $\sigma$  bonds of length  $a = 1.421\text{\AA}$ . These bonds are responsible for the mechanical properties of graphene. In addition to these three orbitals, one orbital that is perpendicular to the plane formed by carbon atoms forms a  $\pi$  bond. These  $\pi$  orbitals play an important role in the electronic properties of graphene. One unit cell of graphene layer contains 2 distinct carbon atoms, say A and B (Fig.2.2)

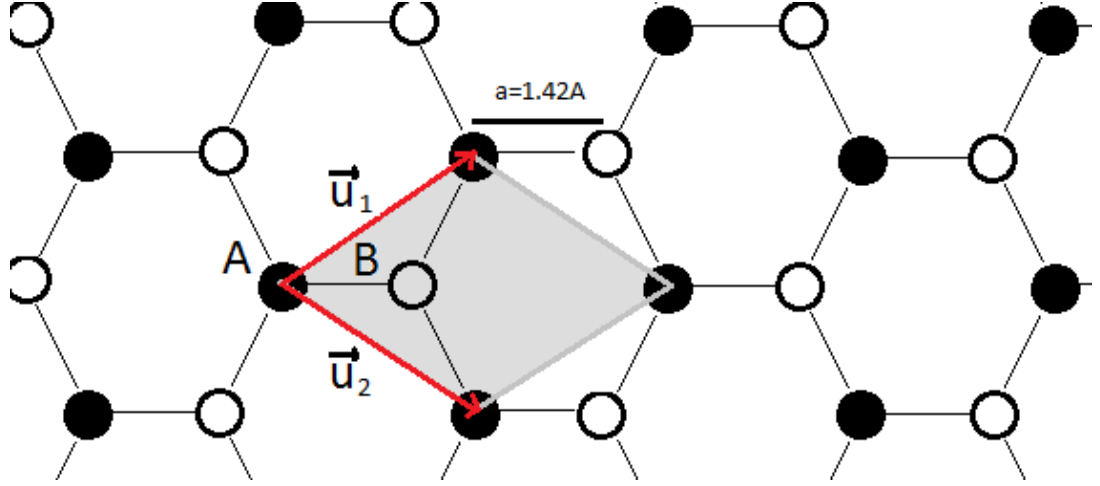


Figure 2.2: Unit cell of graphene

The energy spectrum contributed by the  $\pi$ -orbitals has two bands, named the valence and the conduction bands and denoted with the symbols  $\pi$  and  $\pi^*$ , respectively. Graphene has a half filled band structure; consequently, the valence band is completely filled. These energy bands can be calculated using tight binding method, which uses a set of wave functions generated by the superposition of localized atomic orbitals [32]. Conduction and valence bands including the first nearest neighbor of carbon-carbon interactions of  $\pi$ -orbitals of single graphene sheet is formulated with the TB method in this form:

$$E_{v,c}(k_x, k_y) = \frac{\epsilon \pm t \sqrt{1 + 4 \cos\left(\frac{\sqrt{3}k_x a}{2}\right) \cos\left(\frac{k_y a}{2}\right) + 4 \cos^2\left(\frac{k_y a}{2}\right)}}{1 \pm s \sqrt{1 + 4 \cos\left(\frac{\sqrt{3}k_x a}{2}\right) \cos\left(\frac{k_y a}{2}\right) + 4 \cos^2\left(\frac{k_y a}{2}\right)}} \quad (2.1)$$

where  $t$  is the TB hopping parameter (overlap integral between  $\pi$ -orbitals),  $\epsilon$  is the on-site energy parameter, both expressed in electron-volts (eV), and  $s$  is the unitless overlap parameter.  $a$  is the lattice parameter of graphene, and  $(k_x, k_y)$  represents the 2D wavevector components

along the x and y directions in the 2D Brillouin zone of graphene.

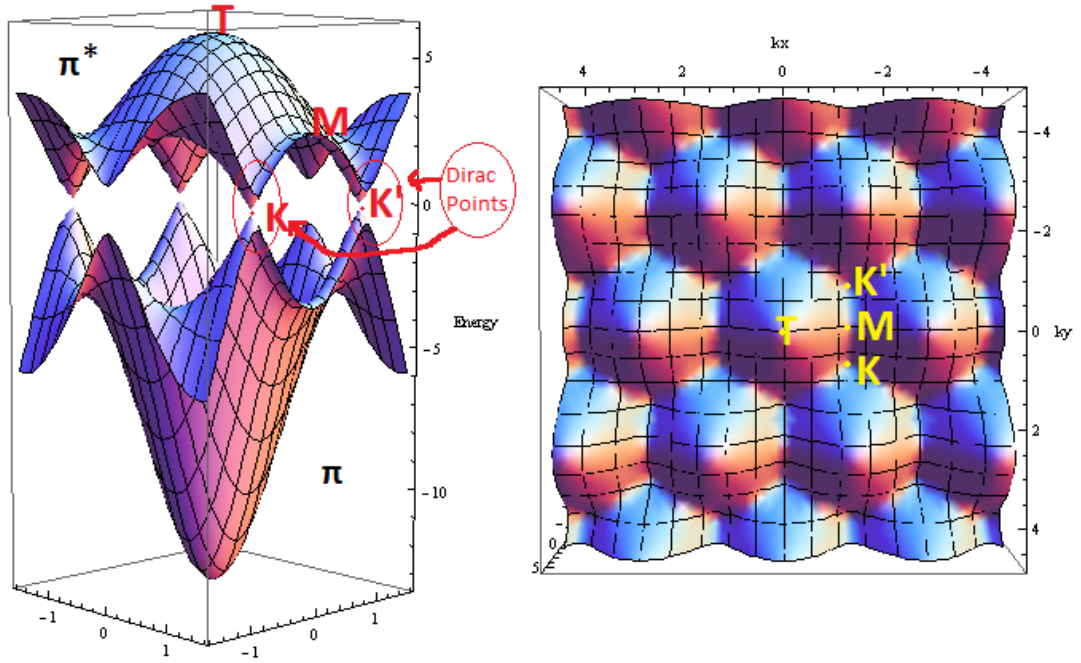


Figure 2.3: Energy band dispersion and Brillouin zone of graphene

Electrons described by Bloch wavefunctions have an 'effective mass' in a solid, which can be different than the free electron mass. If we denote group velocity by  $v$ , momentum by  $p$ , and force by  $F$ , it can be derived in this way:

$$v = d\omega/dk = \frac{1}{\hbar} \frac{d\varepsilon}{dk} \quad (2.2)$$

$$F = d\mathbf{p}/dt = \hbar \frac{dk}{dt} \quad (2.3)$$

$$F = m^* \frac{dv}{dt} = m^* \frac{1}{\hbar} \frac{d^2\varepsilon}{dk^2} \frac{dk}{dt} \quad (2.4)$$

$$\Rightarrow m^* = \frac{1}{\hbar^2} \frac{d^2\varepsilon}{dk^2} \quad (2.5)$$

Electrical properties of solids, such as being a metal or a semiconductor, depends on this effective mass. Density of states at the Fermi energy vanishes near zero energy in graphene, and electrons show a massless behavior; therefore, they obey the Dirac Equation [31]. In other word, the velocity does not depend on the mass. Consequently, the relationship between the

energy and the momentum is given by  $E = v_f P$ . velocity is called Fermi velocity,  $v_f$  and it is approximately  $1 \times 10^6$  m/s. Interestingly, only a honeycomb lattice produces this peculiar energy-momentum relationship. Electrons in other two dimensional periodic structures, such as square or triangular lattices have a non-zero effective mass [33]. It is clear from Fig.2.3 that the valance and the conduction bands touch each other at particular momentum values referred to as Dirac points. Graphene is sometimes referred to as a 'zero gap semiconductor' because of the vanishing density of states at the Fermi energy[31].

## 2.1 GRAPHENE LAYERS

Graphene layers are found to be stacked naturally in 3 ways, AA, AB, and AC stackings. A, B, and C names are chosen according to the position. Atoms of layer B are positioned in the center of hexagon of layer A. An arrangement that corresponds to ABA stacking is called Bernal stacking, and ABC stacking is called rhombohedral stacking as shown in (Fig.2.4) For the 2 layer graphene, AB and AC stackings are the same.

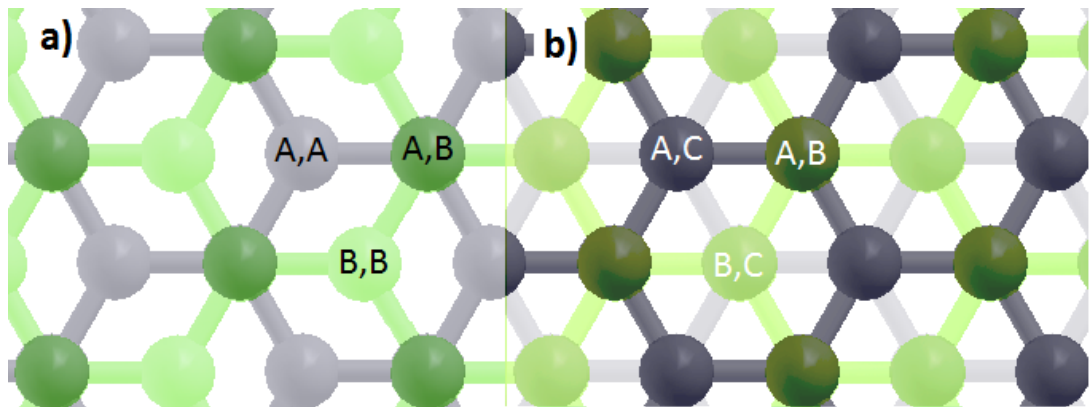


Figure 2.4: **a)** Bernal Stacking **b)** Rombohedral Stacking (A is grey first layer; B is green second; C is light grey third layer)

The presence of a second layer of graphene changes the electronic properties. Bilayer graphene behaves again like a semi-metal; however, its dispersion relation is quadratic, and the charge carriers have nonzero effective masses in the AB stacked bilayer. Electronic band structures are very different for ABC and ABA stacked graphnes. In the Bernal stacked graphene, electronic bands overlap because of symmetry, while the bandgap between the valance and the

conduction bands is formed in the presence of electric field in the rhombohedral stacking. This has been also proved experimentally [34] : Figure 2.5 shows the bias voltage vs. measured resistance graphs at different top gate voltages and band diagrams of (a,b) ABC and (c,d) ABA trilayers. Part (a) shows that in the ABC layers, the resistance increases with decreasing top gate voltage. On the other hand, part (c) shows that the resistance is lower in ABA stacked layers at the same back-gate bias levels, even with lower top gate voltages. From these results, it can be concluded that the resistance of the material increases in ABC stacking and decreases in ABA stacking, with the applied electric field.

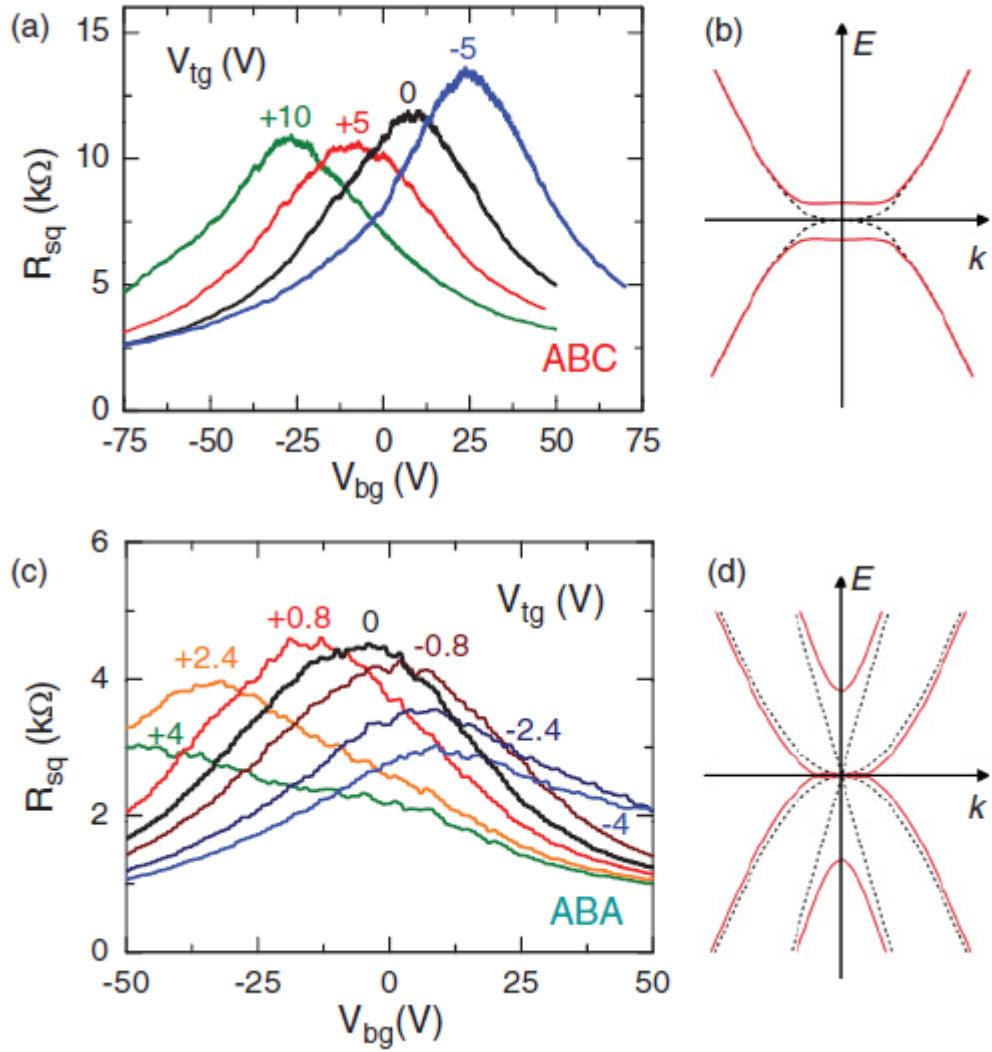


Figure 2.5: Bias voltage vs. measured resistance graphs at different top gate voltages and band diagrams of (a, b) ABC, and (c, d) ABA trilayers. The ABC and ABA trilayers are separated from the top gate by 90 nm and 15 nm dielectric layers, respectively. The bias voltages are applied from the back gate. The solid and the dashed lines in the energy band diagrams represent the cases with and without an external electric field, respectively. A perpendicular external electrical field results in an energy gap in the ABC trilayer and a band overlap in the ABA trilayer [34].

Electron transport under applied electric field has been investigated by many researchers [34, 35, 36]. Quantum Hall effect is the other property that is shown in graphene under applied magnetic field. Quantized electron energy levels that appears for nonzero magnetic field are called Landau levels. This research is also important for the development of field effect transistors [37]. Besides these properties of the few layer graphene (FLG), an interesting

phenomenon is observed when the layers are twisted: When rotational faults occur, charge carriers behave like massless particles similar to the single layer graphene (SLG) in the linear Dirac points [38]. Electronic properties of a SLG and a FLG with layers rotated more than  $20^\circ$  are indistinguishable from each other. For angles less than  $3^\circ$ , Dirac fermions have renormalized velocities. At very small angles, density of states diverges at saddle points and causes van Hove Singularities instead of Dirac cones [39, 40]. The electronic, optical, vibrational, and transport properties of a rotated layer graphene can be adjusted using a controlled fabrication process.

## 2.2 MOIRE PATTERN

Moire effect is observed when structures are superposed and viewed against each other [41]. Even the slightest displacement may cause a large variations in the pattern, and this phenomenon is used in various kinds of applications. One example of moire pattern, which is caused by the difference of the optical path of the light is used to determine object deformations or slight deflections in strain analysis [42]. It also provides information about very small angles, displacements, and movements of atoms in metrology. Moire patterns are also formed when two layers of graphene are rotated with respect to each other. These periodic structures can be observed by a scanning tunneling microscope (STM): Presence of superlattice structures with a periodic length much larger than the graphene lattice constant, 1.42 Å, in an STM image indicates the presence of moire patterns [43,44,45,46]. High-resolution tunneling electron microscope (HRTEM) is also used for observing moire patterns as given in Fig.2.6 [47]. In Fig.2.6-a, there are 6 layers of graphene and they have an average rotation of 10 degrees with respect to each other. A more clear image of a moire pattern is shown in Fig.2.6-b, which is the part in the blue rectangle in Fig.2.6-a. Fig.2.6-c is the HRTEM image of two layer graphene, and (d) and (e) are parts of the region given in the red rectangle in Fig.2.6-c, where the rotation amount is determined as 7 degrees.

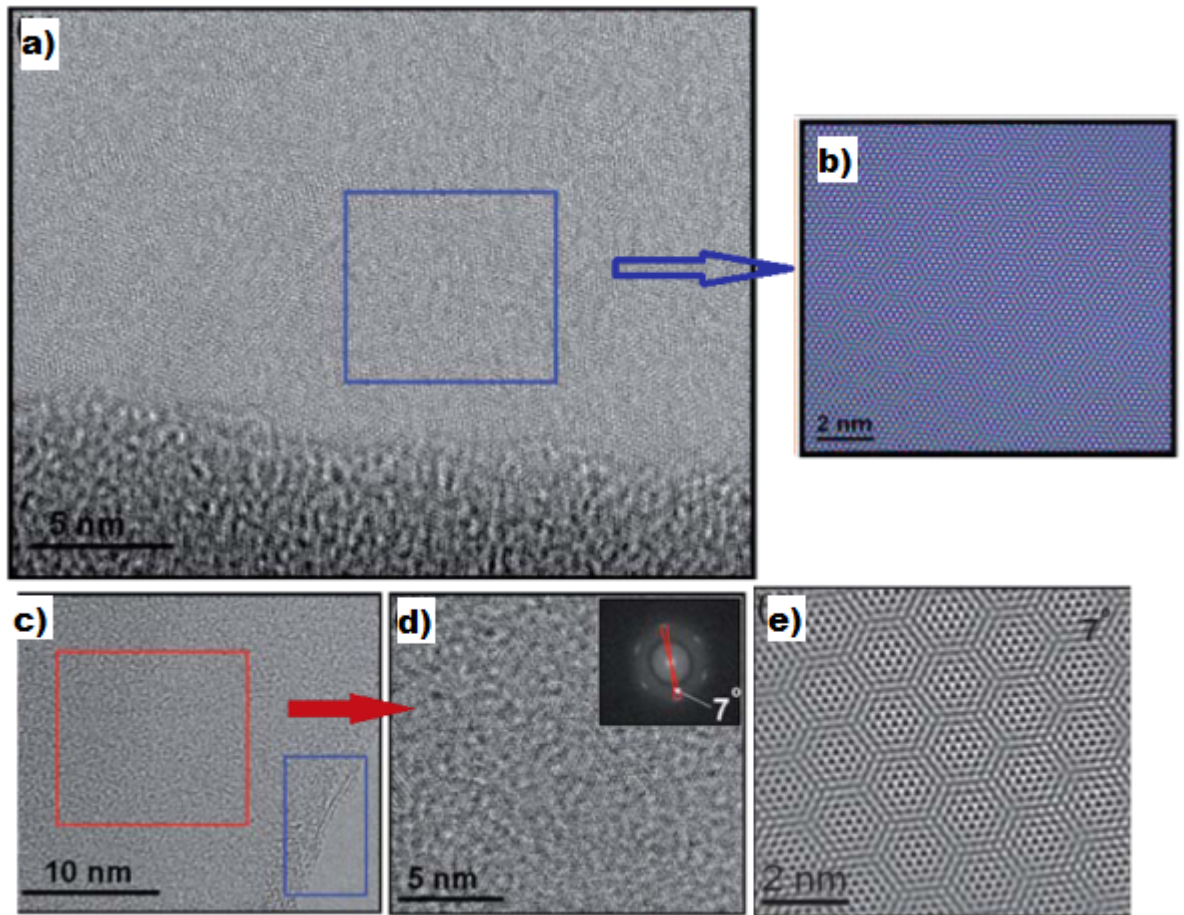


Figure 2.6: Some moiré patterns observed by HRTEM from reference [47].

### 2.2.1 Geometric Investigation of Hexagonal Moiré Patterns

In this study, the shape of the graphene layers are chosen as hexagons in this study, for convenience during the geometric investigation of the moiré patterns. A self-written GNU Octave code was used to generate the hexagonal flakes with a predetermined number of shells around a central atom. Figure 2.7 shows a graphene flake formed using hexagonal layers as described. Enclosing shells are distinguished from each other using red and blue colors in the figure.  $N$  represents the number of these shells, and it also determines the size of the flake, which can be used to calculate the number of atoms in each unit cell of periodic moiré patterns.

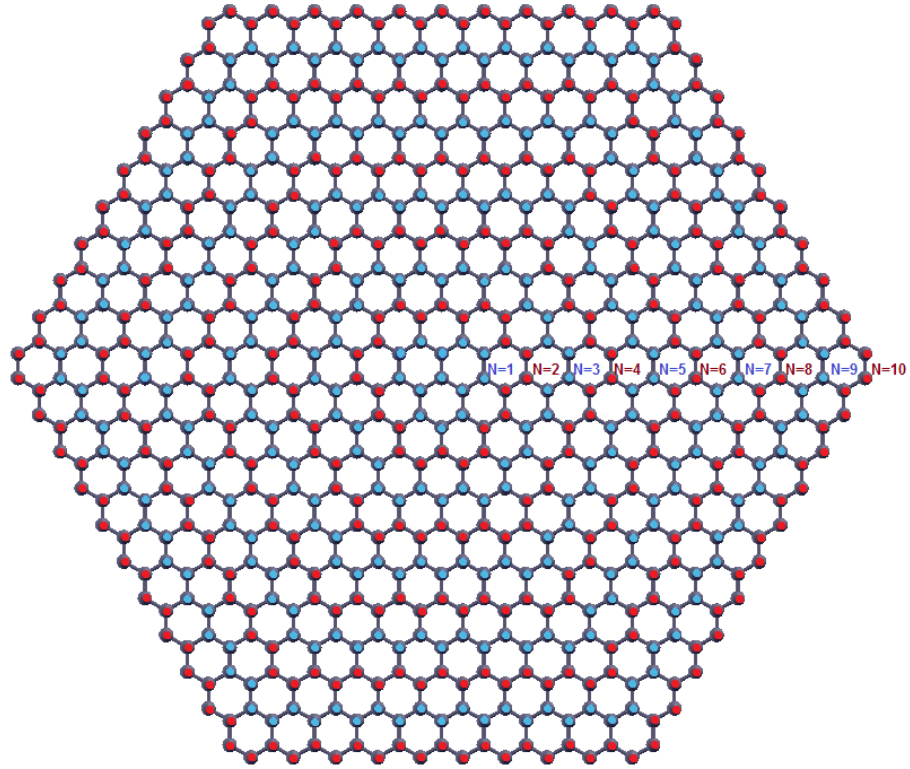


Figure 2.7: Graphene flake is constructed as hexagonal layer represented by  $N$  for each shell

Periodic and non periodic moire patterns can be formed when two honeycomb shaped patterns are rotated with respect to each other. In this thesis, hexagonal honeycomb layers are twisted on each other around the center, which results in patterns formed in hexagonal structures. Some patterns may seem identical to each other although they are not. In order to create a periodic Moire pattern, two atoms should be brought on top of each other by applying a rotation around the center atoms. Consequently, symmetry axes should be determined. When two points at the corners of smallest hexagons, which have same distance to center are brought same point periodic moire patterns occurs. For example, the pattern which includes the maximum number of atoms in a unit cell with  $N = 6$  can be constructed by two symmetric points, which are given in red color in Fig.2.8. As shown in Fig.2.8, there are four zones, two of which are completely symmetric according to the lines,  $y = \frac{1}{\sqrt{3}}x$  and  $y = \frac{-1}{\sqrt{3}}x$ . There are also some points that are symmetric with respect to the  $y = \sqrt{3}x$  line and the  $x$  axis. However, the number of atoms per unit cell increases as the angle is decreased. Consequently,

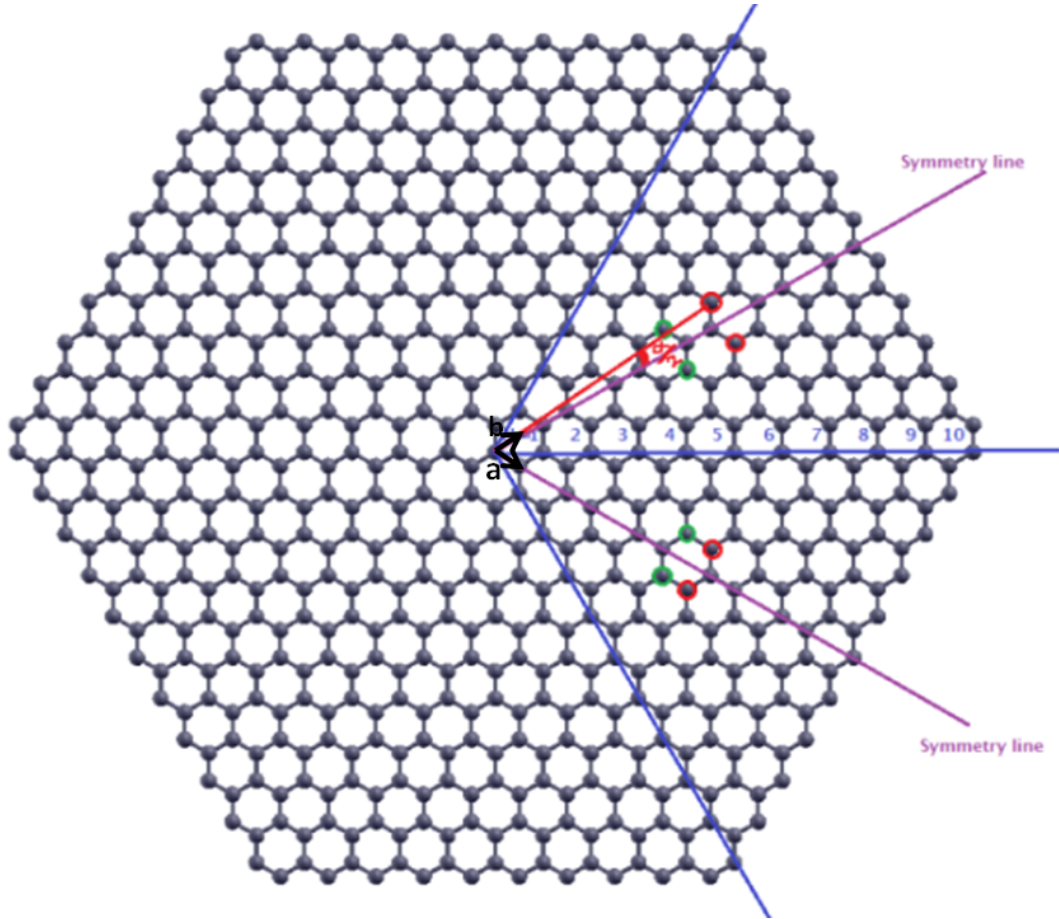


Figure 2.8: To identify periodic moire patterns symmetric points according to the symmetry lines should coincide

the smallest symmetry angles belong to  $y = \frac{1}{\sqrt{3}}x$  and  $y = \frac{-1}{\sqrt{3}}x$ .

The angle required for periodic moire patterns for maximum atoms in a unit cell determined for a specific  $N$  can be written as:

$$\theta = \frac{\alpha}{2} = \begin{cases} \arctan \frac{\sqrt{3}}{3N \pm 1} & , \text{ if } N \text{ is even} \\ \arctan \frac{\sqrt{3}}{3N} & , \text{ if } N \text{ is odd} \end{cases} \quad (2.6)$$

When  $N$  is even, there are two angles for a given  $N$  with respect to the two symmetry lines given in figure (2.8). (+) belongs to the smallest angle between the  $y = \frac{1}{\sqrt{3}}x$  line and the vector from the center atom to the chosen atom closest to the  $y = \frac{1}{\sqrt{3}}x$  line in the first region of the cartesian coordinate system. Similarly, (-) belongs to the angle between  $y = \frac{-1}{\sqrt{3}}x$

and the vector from the center atom to the chosen atom closest to the  $y = \frac{-1}{\sqrt{3}}x$  line in the fourth region. When  $N$  is odd, there is only one angle required for periodicity for a specific  $N$ . Minimum angles for the specific  $N$  and the number of atoms in these flakes are given in the table (2.1).

Table 2.1: Angles for periodic moire pattern for largest unit cells. # of atoms belong to hexagonal double layers.

N	Angle	# of atoms	N	Angle	# of atoms
1.0000	60.0000	26	16.0000	4.0489	3266
2.0000	27.7958	74	16.0000	4.2210	3266
2.0000	38.2132	74	17.0000	3.8902	3674
3.0000	21.7868	146	18.0000	3.6075	4106
4.0000	15.1782	242	18.0000	3.7435	4106
4.0000	17.8966	242	19.0000	3.4810	4562
5.0000	13.1736	362	20.0000	3.2529	5042
6.0000	10.4174	506	20.0000	3.3631	5042
6.0000	11.6351	506	21.0000	3.1497	5546
7.0000	9.4300	674	22.0000	2.9617	6074
8.0000	7.9265	866	22.0000	3.0528	6074
8.0000	8.6132	866	23.0000	2.8759	6626
9.0000	7.3410	1082	24.0000	2.7184	7202
10.0000	6.3959	1322	24.0000	2.7949	7202
10.0000	6.8360	1322	25.0000	2.6459	7802
11.0000	6.0090	1586	26.0000	2.5120	8426
12.0000	5.3604	1874	26.0000	2.5772	8426
12.0000	5.6662	1874	27.0000	2.4500	9074
13.0000	5.0858	2186	28.0000	2.3347	9746
14.0000	4.6133	2522	28.0000	2.3910	9746
14.0000	4.8381	2522	29.0000	2.2811	10442
15.0000	4.4085	2882	30.0000	2.1808	11162
			30.0000	2.2298	11162

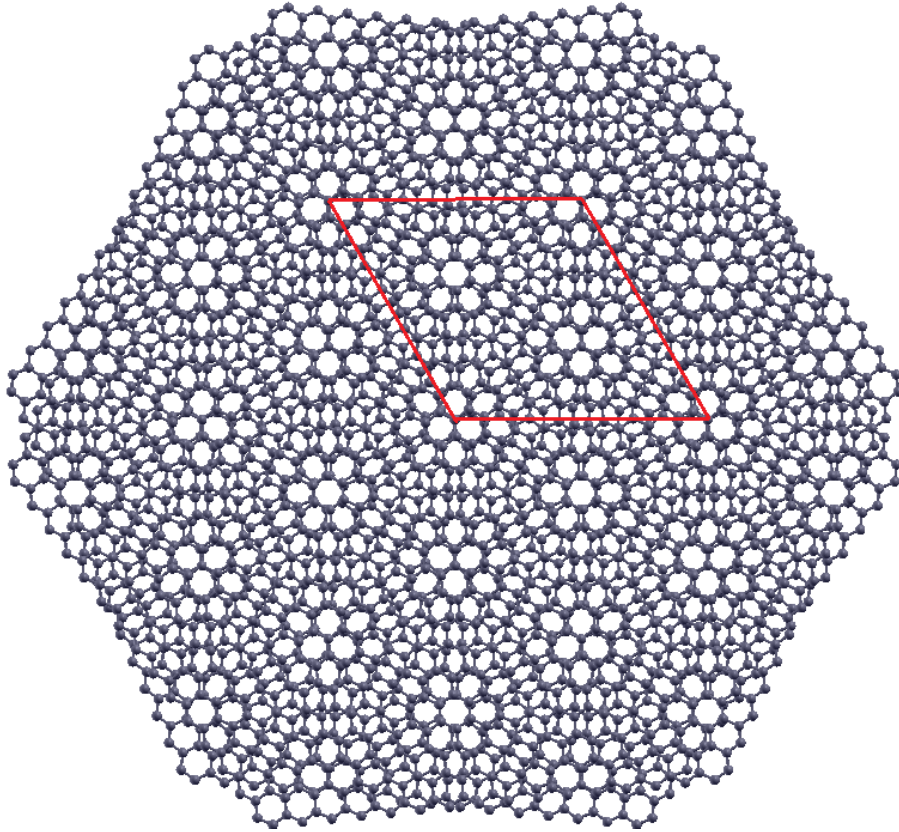


Figure 2.9: Periodic moire pattern is constructed when the atoms are eclipsed at  $N=6$  with  $\alpha = 10.4174$

The condition for periodicity of a moire pattern can also be written in vectorial form.[48]. For this notation, two basis vectors should be chosen.  $\mathbf{a}$  and  $\mathbf{b}$  denote these vectors in Figure 2.8. In this case, the position of the chosen atom can be described by a vector  $\mathbf{V} = m\mathbf{a} + n\mathbf{b}$  where  $n$  and  $m$  are integers. The rotation angle is equal to twice the angle between the vectors  $\mathbf{a}$  and  $\mathbf{V}$  in the fourth region and the angle between the vectors  $\mathbf{b}$  and  $\mathbf{V}$  in the first region.  $m$  is greater than  $n$  if  $\vec{V}$  represents an atom in the first region of the coordinate system, and it is less than  $n$  if  $\vec{V}$  represents an atom in the fourth region. The periodicity condition with respect to

the  $y = \frac{-1}{\sqrt{3}}x$  line depends on the angle between  $\vec{V}$  and  $\vec{d}$ , which can be found as shown below:

$$\vec{V} = m\vec{a} + n\vec{b} \quad (2.7)$$

$$\vec{d} = \sqrt{3}\widehat{d}i - \widehat{d}j \quad (2.8)$$

$$\vec{b} = \sqrt{3}\widehat{d}i + \widehat{d}j \quad (2.9)$$

$$\vec{V} \cdot \vec{d} = V.a. \cos \frac{\alpha}{2} = d \sqrt{3(m+n)^2 + (m-n)^2} \cdot 2d \cdot \cos \frac{\alpha}{2} \quad (2.10)$$

$$\vec{V} \cdot \vec{d} = m.\vec{a} \cdot \vec{d} + n\vec{b} \cdot \vec{d} = m.2d.2d + n.2d.2d \cdot \cos 60 \quad (2.11)$$

$$\Rightarrow \cos \frac{\alpha}{2} = \frac{2m+n}{2\sqrt{m^2+n^2+m.n}} \quad (2.12)$$

$$\Rightarrow \tan \frac{\alpha}{2} = \frac{n\sqrt{3}}{2m+n} \quad (2.13)$$

The same calculation can be done to find the periodicity condition with respect to the  $y = \frac{-1}{\sqrt{3}}x$  line, only this time by using the angle between  $\vec{V}$  and  $\vec{b}$ . With  $n > m$  :

$$\frac{\alpha}{2} = \arctan\left(\frac{m\sqrt{3}}{2n+m}\right) \quad (2.14)$$

which is the same result as Eq.(2.14). Thus, we conclude that this condition is the general rule for the periodicity of a moire pattern for any point described by a vector  $\mathbf{V} = m\mathbf{a} + n\mathbf{b}$ . If there is an atom position described by  $\mathbf{V}' = n\mathbf{a} + m\mathbf{b}$ , this means that these points are symmetric with respect to x axis, and also the rotation period is  $60^\circ$ . If there are no atoms that are symmetric with respect to the x axis, then the rotation period is  $120^\circ$ .

The vector  $\vec{V}$  can also be described in terms of N for the last shell of points as follows:

Zone	$\vec{V}$
on x axis	$N\vec{a} + N\vec{b}$
1	$(N - 1)\vec{a} + (N + 1)\vec{b}$
1	$(N - 2)\vec{a} + (N + 1)\vec{b}$
1	$(N - 3)\vec{a} + (N + 2)\vec{b}$
1	$(N - 4)\vec{a} + (N + 2)\vec{b}$
1	$(N - 5)\vec{a} + (N + 3)\vec{b}$
1	$(N - 6)\vec{a} + (N + 3)\vec{b}$
	$\vdots$
1	$\vec{a} + (\frac{3N}{2} - \frac{1}{2})\vec{b}$ (if N is odd) $\vec{a} + (\frac{3N}{2} - 1)\vec{b}$ (if N is even)
on line $y = \frac{1}{\sqrt{3}}x$	$(\frac{3N}{2} + \frac{1}{2})\vec{b}$ (if N is odd) $(\frac{3N}{2})\vec{b}$ (if N is even)
4	$N\vec{a} + (N - 1)\vec{b}$
4	$(N + 1)\vec{a} + (N - 2)\vec{b}$
4	$(N + 1)\vec{a} + (N - 3)\vec{b}$
4	$(N + 2)\vec{a} + (N - 4)\vec{b}$
4	$(N + 2)\vec{a} + (N - 5)\vec{b}$
4	$(N + 3)\vec{a} + (N - 6)\vec{b}$
4	$(N + 3)\vec{a} + (N - 7)\vec{b}$
	$\vdots$
4	$(\frac{3N}{2} - \frac{3}{2})\vec{a} + \vec{b}$ (if N is odd) $(\frac{3N}{2} - 1)\vec{a} + \vec{b}$ (if N is even)
on line $y = \frac{-1}{\sqrt{3}}x$	$(\frac{3N}{2} - \frac{1}{2})\vec{a}$ (if N is odd) $(\frac{3N}{2})\vec{a}$ (if N is even)

## CHAPTER 3

### MOLECULAR DYNAMICS SIMULATION OF GRAPHENE

Two-layer graphene has several features that make it a promising material for the future improvements in nanotechnology. One of the crucial features for a material to be used in nanotechnology is its stability. This study aims to examine the stability of the two-layer graphene using molecular dynamics simulations. LAMMPS (Large-scale Atomic/Molecular Massively Parallel Simulator), which has a GNU general public license, is used for the MD simulations of two layer graphene in this study. Required potential function was chosen as AIREBO (Adaptive intermolecular reactive bond order) potential [49], which is an improved version of REBO (reactive empirical bond order) potential that was initially developed for the simulation of chemical vapor deposition of diamond [50]. REBO includes the Tersoff potential [51], which allows the formation and dissociation of covalent bonds during the simulation. The changes in covalent bonds are modeled empirically rather than using a quantum mechanical approach. REBO potential can be used for bulk systems; however, it does not include the torsional interaction potential or the non-bonded interactions, which is not convenient for close interfaces. AIREBO potential has been developed in order to overcome these problems. It can be written as a sum of pairwise interactions, including covalent bonding (REBO) interactions, Lennard-Jones terms, and torsional interactions:

$$\frac{1}{2} \sum_i \sum_{i \neq j} [E_{ij}^{REBO} + E_{ij}^{LJ} + \sum_{i \neq i, j} \sum_{l \neq i, j, k} E_{k,i,j,l}^{tors}]. \quad (3.1)$$

Important part of this potential for double layer graphene system is REBO potential which refers to covalent bonding between carbon atoms, and the Lennard-Jones term in the AIREBO potential which refers the molecular-molecular interaction (Van der Waals interaction) between layers. Last term is given for torsional interactions in AIREBO potential but it is not used in this thesis because there is not any rotation around a bond. In the simulations performed throughout the course of this thesis, twisting angles and corresponding moire patterns

are searched for stability. The potential energy has also been mapped according to these moire angles. However, this was not an easy process because of sliding of layers on each other. Calculation of rotation angle between the graphene layers are done by taking projection of the neighbour atoms of central atoms with respect to the plane which is perpendicular to the axis passed through the central atoms (Fig.3.1).

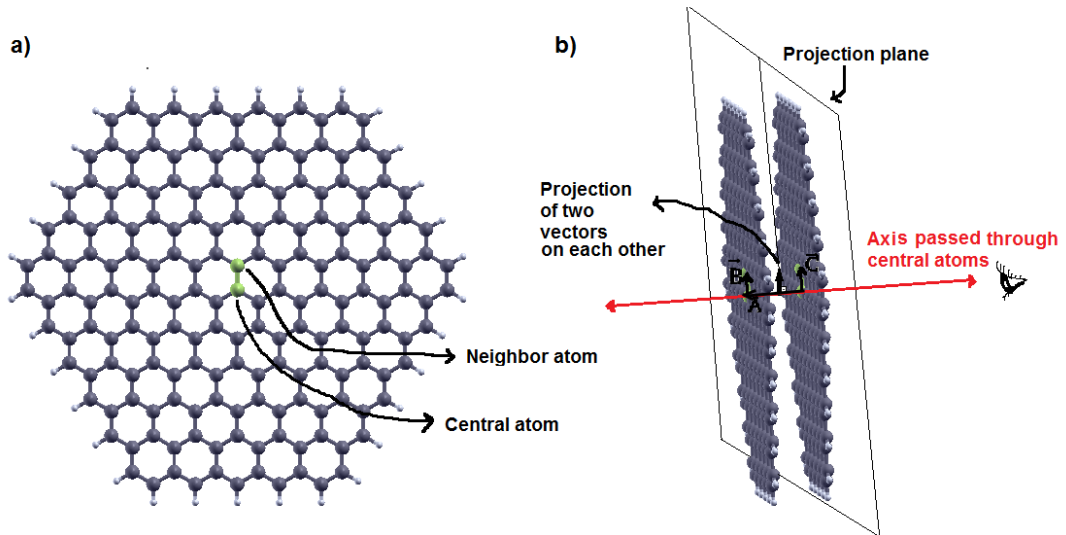


Figure 3.1: a)Two graphene layers with 0 degrees with respect to each other. Central atom and neighbor atom on one layer is showed. b) Vectors from central atom to neighbor atom on both layer. The angle between the projections of these vectors to plane, which is perpendicular to the axis passed through central atoms is 0 degree.

Graphene layers are not completely parallel to each other. One layer can not be on a same plane because of dynamic simulation of phonon modes. Some slight sliding of layers with respect to each others also observed in last simulations. This motion can be eliminated by this calculation. The reference system of this calculation of angle includes coincidence of central atoms positions. Angle calculation is done with home written Octave code by using simple vector algebra, which includes cross product and dot product rules. Associated Octave code for angle calculation part is given in Fig.3.2. By dot product, only length of the vector can be found on some projection plane. On the other hand cross product gives direction of the vectors. The vector from central atom on the first layer to central atom on the second layer is defined by  $\vec{A}$ , the vectors from central atom to neighbor atom on second layer and first layer are defined by  $\vec{B}$  and  $\vec{C}$ . In this code, main idea is angle between each cross product of vectors  $\vec{B}$  and  $\vec{C}$  with the vector  $\vec{A}$  is equal to angle between two projections of vectors  $\vec{B}$  and  $\vec{C}$  on a

```

acilar=[];
for n=0:length(o)/atoms-1
%vector at axis passed through central atoms (from 1st. to 2nd. layer
A=o(1+n*atoms,2:4)-o(662+n*atoms,2:4);
% vector from central atom to neighbour on second layer
B=o(783+n*atoms,2:4)-o(662+n*atoms,2:4);
% vector from central atom to neighbour on first layer
C=o(122+n*atoms,2:4)-o(1+n*atoms,2:4);

%Calculation of unit vector for 90 degrees rotated projection of B on projection plane
v=cross([cross(A,B)],A);
unitv=v/norm(v);
% angle between projection plane and B
alfa1=acos((-A*B')/(norm(A)*norm(B)))-pi/2;
% projected B (rotated 90 degrees)
b=norm(B)*cos(alfa1)*unitv;

%Calculation of unit vector for 90 degrees rotated projection of C on projection plane
v2=cross(A,[cross(C,A)]);
unitv2=v2/norm(v2);
% angle between projection plane and C
alfa2=acos((-A*C')/(norm(A)*norm(C)))-pi/2;
% projected C (rotated 90 degrees)
c=norm(C)*cos(alfa2)*unitv2;

% calculation of angle from dot product
uzunluk=norm(c)*norm(b);
theta=acos((c*b')/uzunluk)*180/pi;
acilar=[acilar;theta];
endfor

```

Figure 3.2: Part of Octave code for calculation of angle.

perpendicular plane to the axis passed through central atoms (Fig.3.1).

Four different types of computational experiments are done in this study: (1) Simply, bringing two hexagonal layers of graphene on top of each other and performing the molecular dynamics simulation, (2) Finding periodic moire patterns and simulation of infinite layers, (3) defining each layer of atoms as a group so that the initial conditions are provided as intended. (4) stretching the graphene from its edge to a rigid body.(This may simulate growth the layer on sample)

### 3.1 EXPERIMENT 1: Hexagonal graphene

For this experiment, graphene layers are prepared with an Octave code as explained in chapter 2. The distance between the hexagonal layers is set as 3.35Å. Carbon atoms at the edge of the flake are bonded with hydrogen to preserve  $sp^3$  hybridization. Atom IDs are used to distinguish different atom types from each other during the simulation in the LAMMPS input. There are two different atom IDs defined in this simulation, one for the carbon and the other for the hydrogen atoms. In the part of LAMMPS input given below, the atom IDs for the

carbon and the hydrogen atoms are 1 and 2, respectively, as defined with the same order in the second line.

```
pair_style airebo 3.4 1 0
pair_coeff * * /home/hande/lammps-9Dec11/potentials/CH.airebo C H
```

The first line defines the cut-off distance for the Lennard Jones potential as 3.4Å, and it also shows that the Lennard-jones term is active (1) and torsional term is inactive (0) for AIREBO potential. Torsional term represents the effect of turning around a bond. Therefore, it is usually required for dihedral angles. This term is 0 because graphene planes are parallel to each other. The atom ID is also used with the velocity initialization command. The following input code line creates a Gaussian distribution for velocity at 100 K. The keyword 'all' makes this distribution effective for all included atom types.

```
velocity all create 100 84756204 dist gaussian
```

Nose-Hoover thermostat is used in all simulations during this study. The simulations performed at a high temperature (fluctuating around 100K) resulted in rotation of the graphene layers with respect to the simulation box as well as to each other, which makes it difficult to observe moire patterns. Therefore, the temperature is decreased to 0.1K in order to be able to observe the behavior of the layers.

In the experiment-1, all atoms share commonly defined initial parameters, such as velocity distribution. The time step is determined as 0.1 femtoseconds. Experiment-1 is performed at 0.1 K using 6 different sized flakes.

The first simulation of experiment-1 includes 1448 atoms, which corresponds to an N value of 10 in the derived shell model. The flakes have two different edge lengths; the length of one edge is 22.13Å and the length of the other one is 24.59Å. Three different initial twisting angles, which are 2, 10, and 15 degrees, are assigned for the first 3 simulations. The twisting angles stabilized at 4.29 degrees for all three initial angles.

In the following three steps, the graphene flake sizes are increased: 2024 atoms, 3884 atoms, and 5288 atoms, which correspond to  $N$  values of 12, 17, and 20, respectively, are used in the simulations. The edge lengths of these flakes are again different within each simulation, and these lengths can be listed as 27.05Å- 29.51Å, 39.35Å- 41.82Å, and 46.73Å- 49.19Å, respectively. In the 2024-atom simulation, the twisting angle starts from an initial value of 20 degrees and stabilizes at 3.62 degrees. In the 3884-atom simulation, the angle starts from 10 degrees, rapidly falls down to 5 degrees, and then stabilizes at 2.59 degrees. Finally, in the 5288-atom simulation, the twisting angle starts from 5 degrees and it stabilizes at 4.53 degrees after 700 ps. Table 3.1 presents the summary of the results of experiment-1.

Table 3.1: Summary of the results of experiment-1.

Simulation Time(ps)	Number of Atoms	Initial Angle	Final Angle
1970	1448	2	4.29
970	1448	10	4.29
1450	1448	15	4.29
890	2024	20	3.62
1240	3884	10	2.59
146	5288	5	4.54

### 3.1.1 Graphene Flake With 1448 Atom at 0.1K

1448 atoms are simulated at a nominal temperature of 0.1 K using different initial twisting angles: 2 degrees for the first (Fig.3.6), 10 degrees for the second (Fig.3.22) , and 15 degrees for the third simulation. The final twisting angles obtained at the equilibrated stages of these simulations are very close to each other. Table 3.2 shows the changes in the twisting angle in every 100000 steps for all three simulations, where the time step is determined as 0.0001 picoseconds. In the first step velocity corresponding to temperature of 100K is assigned. Then temperature falls down quickly with heat bath of Nose-Hoover thermostat. The angles given in table 3.2 are found by calculating the angle between the third atoms, which are the neighbors of the central atoms around which the rotation takes place, in each graphene layer on the xy plane. This calculation is performed using GNU Octave, and the corresponding graphs are given in the Fig.3.7, Fig.3.4 and Fig.3.8.

Table 3.2: Experiment1 with 1448 Atoms at OK

Time(x10ps)	Angle1	PE1(eV)	Angle2	PE2(eV)	Angle3	PE3(eV)
1	10.00000	-10623.605	2.000000	-10623.499	15.000000	-10623.459
2	8.629175	-10653.770	4.296010	-10653.882	13.197657	-10653.650
3	8.019817	-10653.733	4.293939	-10653.848	11.465644	-10653.703
4	7.344194	-10653.807	4.292418	-10653.826	9.246924	-10653.749
5	5.274036	-10653.829	4.292389	-10653.867	8.347894	-10653.796
6	4.305265	-10653.893	4.292429	-10653.849	7.798030	-10653.764
7	4.292366	-10653.866	4.292539	-10653.901	6.850461	-10653.767
8	4.292284	-10653.851	4.292580	-10653.873	4.519279	-10653.893
9	4.292347	-10653.863	4.292580	-10653.856	4.294456	-10653.911
10	4.292415	-10653.895	4.292690	-10653.853	4.292425	-10653.870
11	4.292522	-10653.907	4.292730	-10653.865	4.292425	-10653.831
12	4.292545	-10653.896	4.292730	-10653.913	4.292436	-10653.855
13	4.292652	-10653.859	4.292730	-10653.910	4.292542	-10653.888
14	4.292757	-10653.847	4.292740	-10653.865	4.292645	-10653.909
15	4.292757	-10653.879	4.292748	-10653.846	4.292709	-10653.925
16	4.292675	-10653.910	4.292748	-10653.883	4.292660	-10653.897
17	4.292675	-10653.898	4.292881	-10653.925	4.292660	-10653.854
18	4.292783	-10653.881	4.292881	-10653.886	4.292762	-10653.840
19	4.292887	-10653.851	4.292881	-10653.844	4.292762	-10653.880
20	4.292887	-10653.862	4.292881	-10653.851	4.292868	-10653.930
21	4.292887	-10653.889	4.292881	-10653.913	4.292868	-10653.903
22	4.292887	-10653.918	4.292881	-10653.913	4.292868	-10653.844
23	4.292887	-10653.905	4.292881	-10653.854	4.292826	-10653.870
24	4.292887	-10653.851	4.292881	-10653.861	4.292826	-10653.927
25	4.292887	-10653.871	4.292881	-10653.923	4.292826	-10653.882
26	4.292887	-10653.928	4.292881	-10653.894	4.292826	-10653.843
27	4.292887	-10653.894	4.292881	-10653.845	4.292826	-10653.913
28	4.292887	-10653.853	4.292881	-10653.906	4.292929	-10653.908
29	4.292887	-10653.913	4.292881	-10653.913	4.292929	-10653.844
30	4.292887	-10653.904	4.292881	-10653.845	4.292929	-10653.909
31	4.292887	-10653.846	4.292881	-10653.910	4.292929	-10653.908
32	4.292887	-10653.907	4.292991	-10653.905	4.292929	-10653.844
33	4.292850	-10653.904	4.292881	-10653.841	4.292929	-10653.919
34	4.292850	-10653.851	4.292991	-10653.922	4.292929	-10653.890
35	4.292850	-10653.922	4.292991	-10653.883	4.292929	-10653.854
36	4.292850	-10653.880	4.292991	-10653.862	4.292929	-10653.932
37	4.292850	-10653.864	4.292991	-10653.931	4.292929	-10653.853
38	4.292850	-10653.930	4.292991	-10653.847	4.292929	-10653.894
39	4.292850	-10653.852	4.292991	-10653.907	4.292929	-10653.911
40	4.292850	-10653.906	4.292991	-10653.897	4.292929	-10653.847

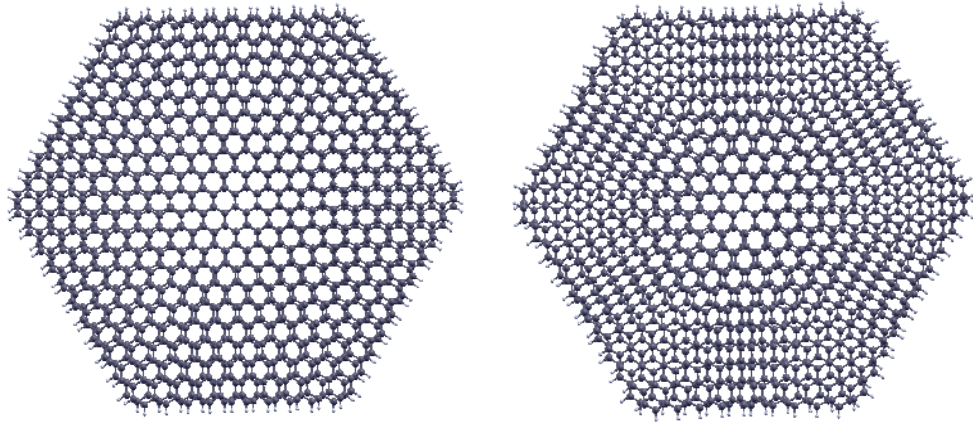


Figure 3.3: The image at the left side shows the initial moiré pattern constructed with a 2-degree twist of graphene flakes. The image at the right side shows the same flake after 1.96 nanoseconds. The simulation is performed at approximately 0 K, and the final rotation angle is 4.29 degrees.

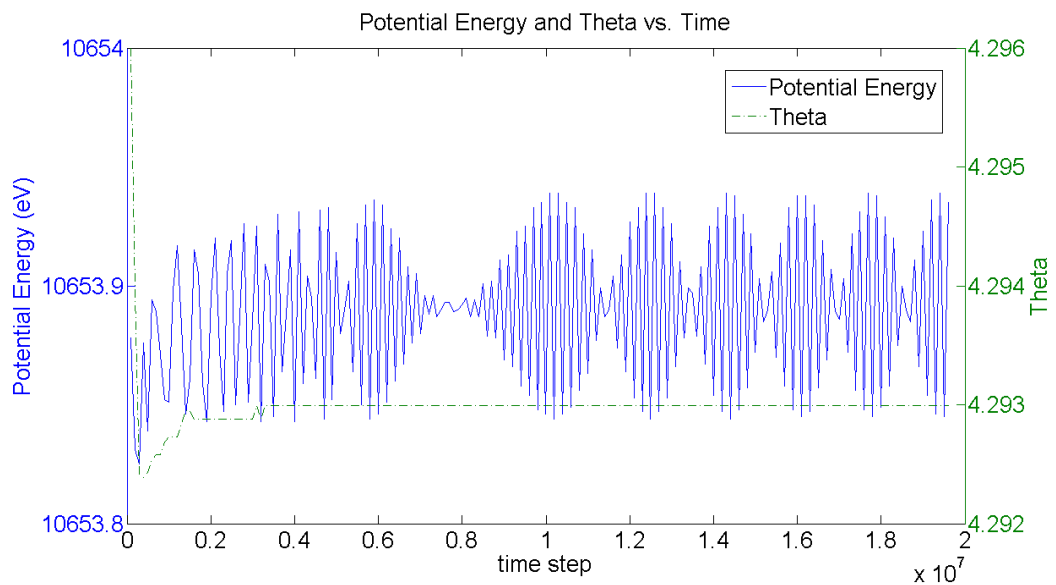


Figure 3.4: The change in the potential energy and the moiré angle with time, which includes 1448 atoms (1332 of them are carbon) and has an initial twisting angle of 2 degrees but initial values did not taken into graph. The final angle stabilizes around 4.29 degrees.

Sampling of the energy selects some specific phonon modes. Calculation of angle is done for each 100000 time step (10ps), frequency of  $10^{11}$  Hz. Therefore, the wave envelope is seen in potential energy graph at Fig.3.4. On the other side, the energy data is recorded with frequency

of  $10^{13}$  Hz. Graph potential energy, kinetic energy and total energy with the sampling of each 1ps, frequency of  $10^{12}$ Hz is given in Fig.3.5

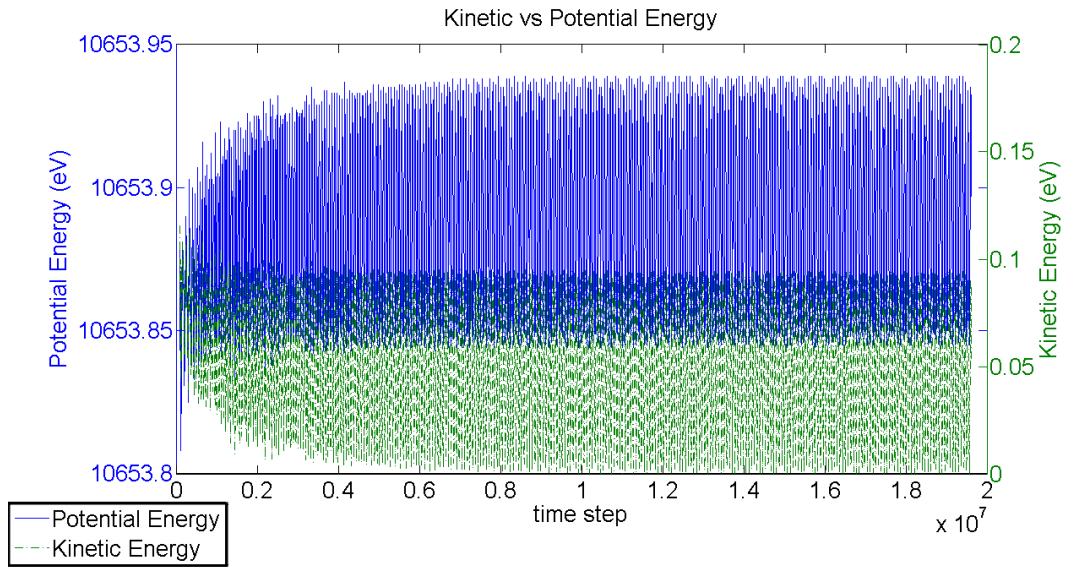


Figure 3.5: The change in the potential energy (blue) and kinetic energy (green) with sampling frequency of  $10^{13}$  Hz for graphene layer with 1448 atoms initial and final twisting angles are 2 and 4.29 respectively.

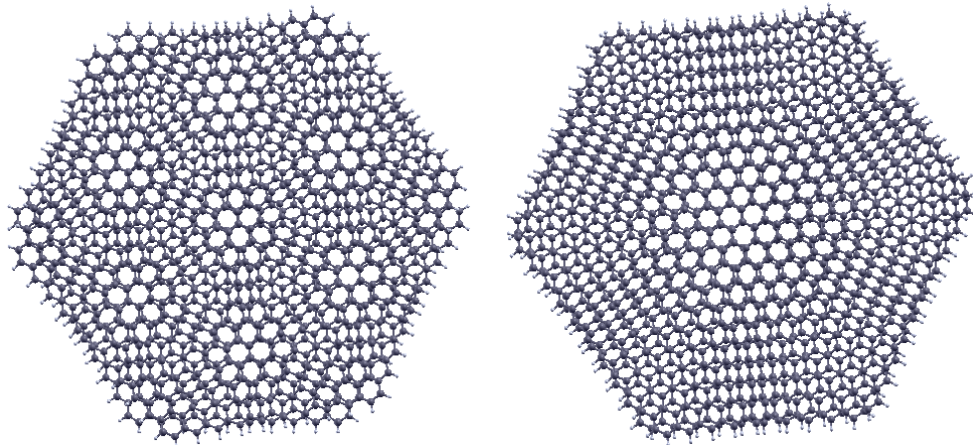


Figure 3.6: The image at the left side shows the initial moire pattern constructed with a 10-degree twist of graphene flakes. The image at the right side shows the same flake after 0.97 nanoseconds. The simulation is performed at approximately 0 K, and the final twist amount is 4.29 degrees.

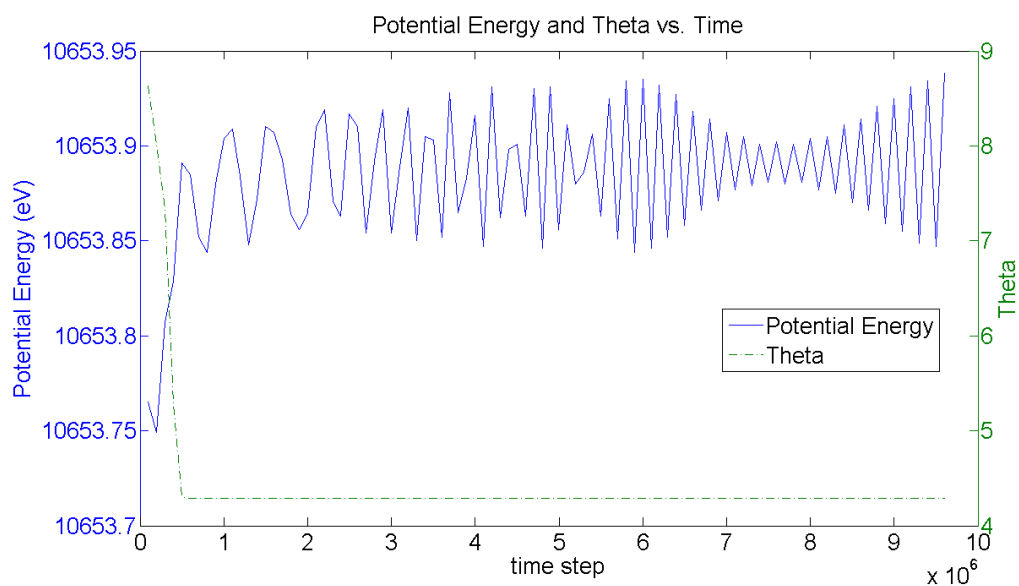


Figure 3.7: The change in the potential energy and the moire angle with time in simulation 1, which includes 1448 atoms (1332 of them are carbon) and has an initial twisting angle of 10 degrees. The final angle stabilizes around 4.29 degrees.

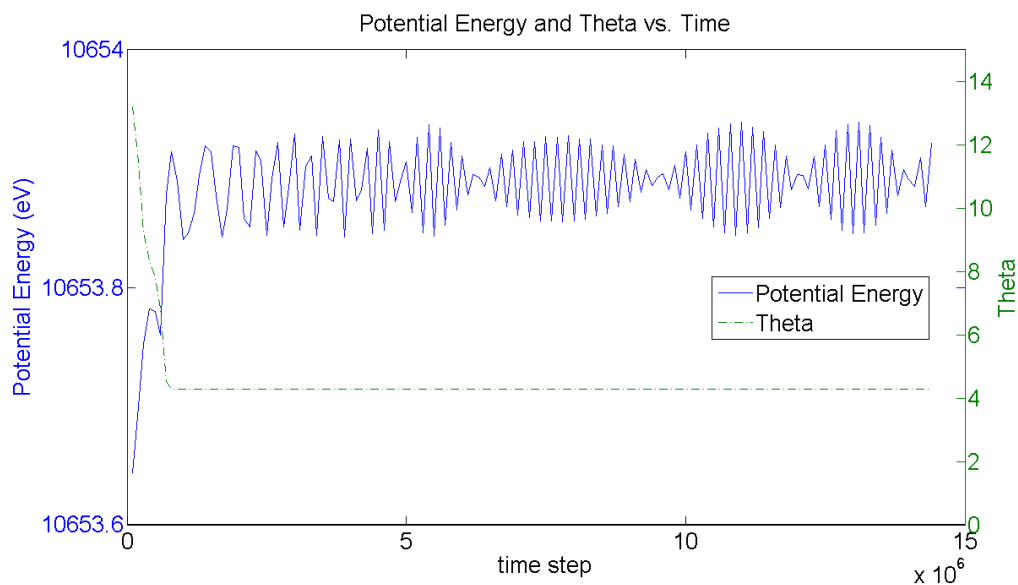


Figure 3.8: The change in the potential energy and the moire angle with time in simulation 3, which includes 1448 atoms (1332 of them are carbon) and has an initial twisting angle of 15 degrees. The final angle again stabilizes around 4.29 degrees.

The obtained results show that the moire patterns with a twist angle of 4.29 degrees are stable,

and the initial angle does not have an effect on this value.

### 3.1.2 Graphene Flake With 2024 Atoms at 0K

In this step, the effect of the size on the final angle, which is described in the previous section, is discussed. For this purpose, the number of atoms is increased from 1448 to 2024, and the simulation is repeated at around 0 K using an initial twist angle of 20 degrees. Final angle is 3.6 degrees. Figure 3.9 shows the result of this simulation.

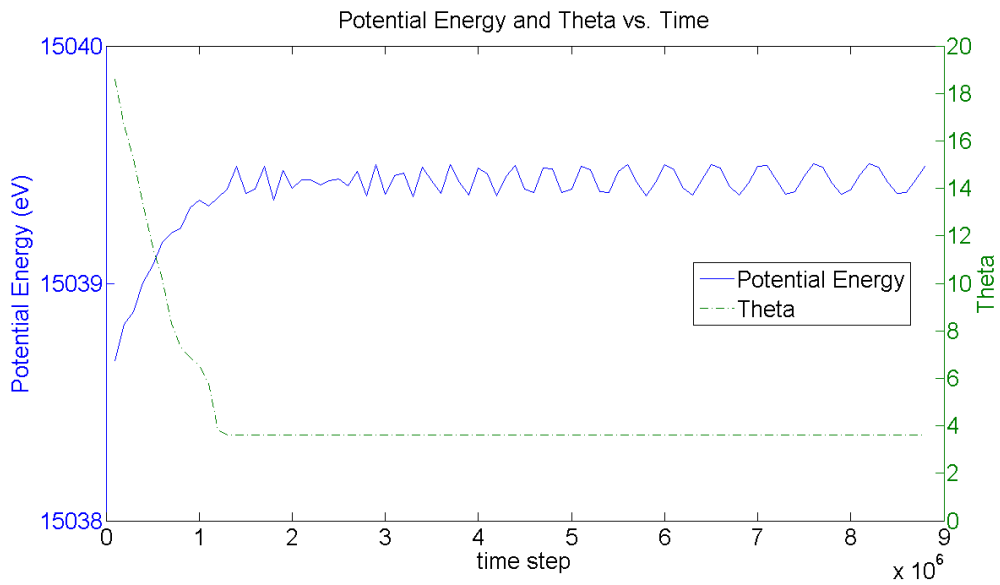


Figure 3.9: The change in the potential energy and the moire angle with time, as obtained for a 2024-atom setup with an initial twisting angle of 20 degrees (initial value not included). The twisting angle stabilizes around 3.62 degrees.

### 3.1.3 Graphene Flake With 3884 Atoms at 0K

In this step the number of atoms is increased from 2024 to 3884, and the simulation is repeated at around 0 K using an initial twist angle of 10 degrees. Figure 3.10 shows the result of this simulation.

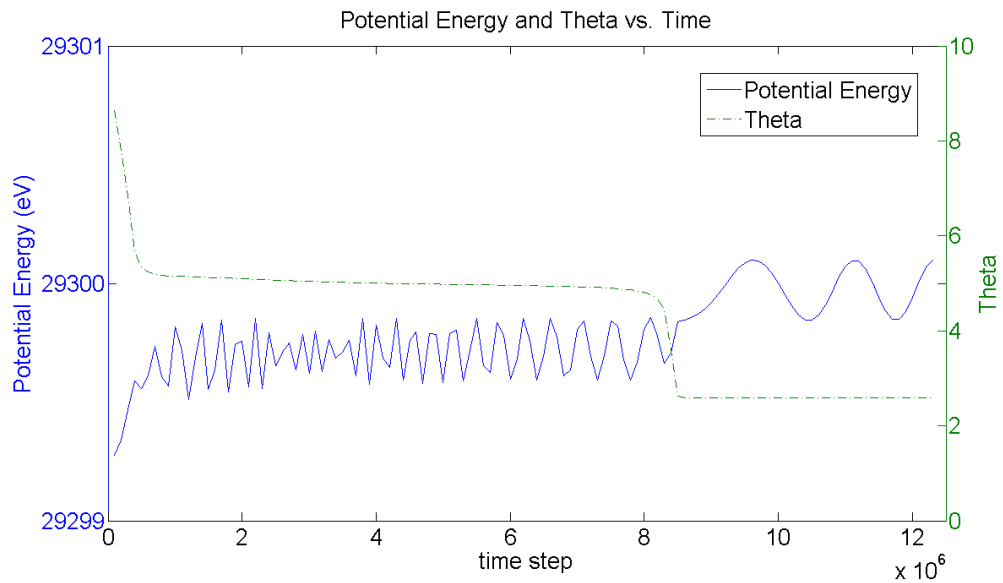


Figure 3.10: The change in the potential energy and the moire angle with time, as obtained for a setup with 3884 atoms and an initial twisting angle of 10 degrees. The final angle becomes 2.59 degrees in this case.

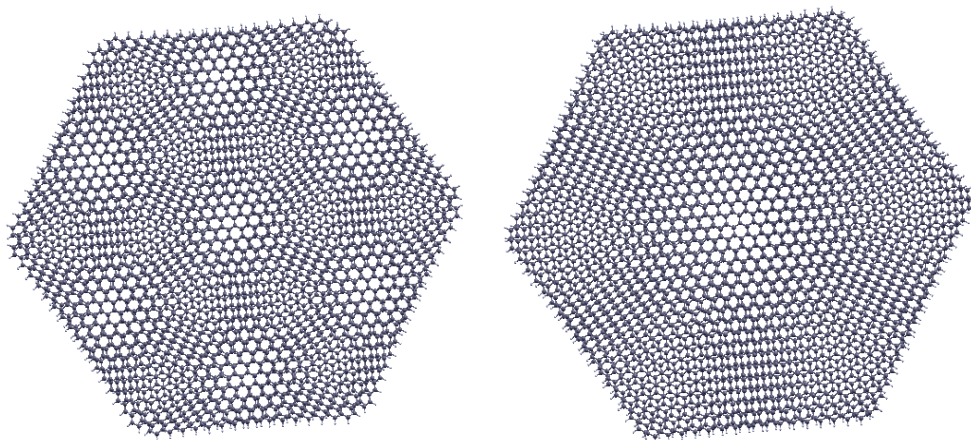


Figure 3.11: Metastable states for the flake with 3884 atoms. The image at the left side shows the angle of 5 degrees. The image at the right side shows the same flake at angle of 2.6 degrees.

In the 4th simulation, the twisting angle starts from 10 degrees and becomes stable at 2.59 degrees at around the time step of 8,800,000 where time step is  $10^{-4}$  ps. After this simulation, the number of atoms is increased to 5288.

### 3.1.4 Graphene Flake With 5288 Atoms at 0K

In this section, a double layer flake corresponding to edges sizes of 46.73Å- 49.19Å and including 5288 atoms is studied. For this purpose, a fifth simulation is added, where the twisting angle starts from 5 degrees and fluctuates around 4.54 after approximately 6,500,000 time steps. The angle stabilizes at 4.536 degrees at the time step of 11,000,000 (1.1ns).

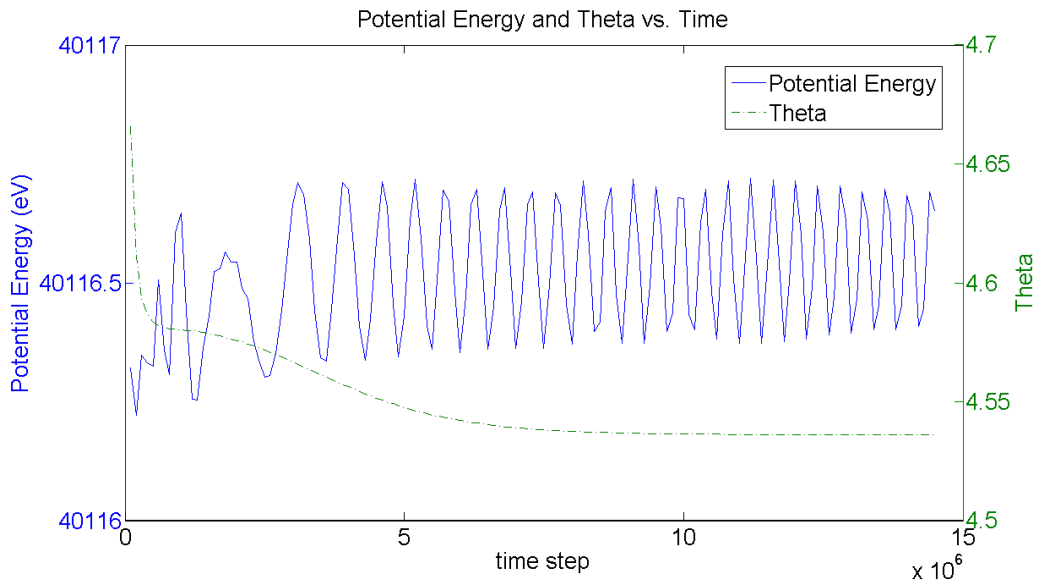


Figure 3.12: The change in the potential energy and moire angle with time, as obtained from last simulation of experiment 1 where the graphene flake has 5288 atoms with an initial twisting angle of 5 degrees. This simulation is performed at around 0K.

## 3.2 EXPERIMENT 2: Periodic Moire Layers

In this experiment, the system boundary is decided to be periodic in xy plane. Periodicity of z axis is selected much more larger than the distance between the graphene layers. As discussed in the previous chapter, some conditions must be satisfied to form periodic moire patterns. In this section, these conditions are enforced with some periodic rectangle layers, which are obtained according to the rules given in chapter 2. Periodic patterns represent infinitely large graphene patterns. Therefore, edge effects are eliminated. By definition, angular momentum becomes always zero with respect to z axis. In the first simulations, all of the assigned atom IDs in LAMMPS code are same. Therefore, the velocity is assigned with a Gaussian distribu-

tion to the atoms of both layers at the same time. However, sliding of layers with respect to each other is observed. Due to initialization problems of the LAMMPS, the velocity of second layer is in the opposite direction of the velocity of the first layer. In order to fix this problem, layers are identified with different atom IDs. In the next step, initial velocities with a Gaussian distribution are separately assigned to each layer in the input. Potential energy for all moire patterns seems to be the same. Total energy and potential energy graphs for 6 different kinds of periodic moire patterns, where initial input parameters are applied to all atoms together, are given in Fig.3.13. The blue line in the graph is for 5.08-degrees twisted periodic layers with 1016 atoms, the red line is for 6-degrees twisted periodic layers with 1456 atoms, the pink line is for 21.79-degrees twisting layers with 1176 atoms, the yellow line is for 27.79-degrees twisted layers with 1248 atoms, the black line is for 38.2-degrees twisted layers with 840 atoms, and the green line is for 13.17-degrees twisted layers with 608 atoms. The thermostat is brought from 100K to 300K.

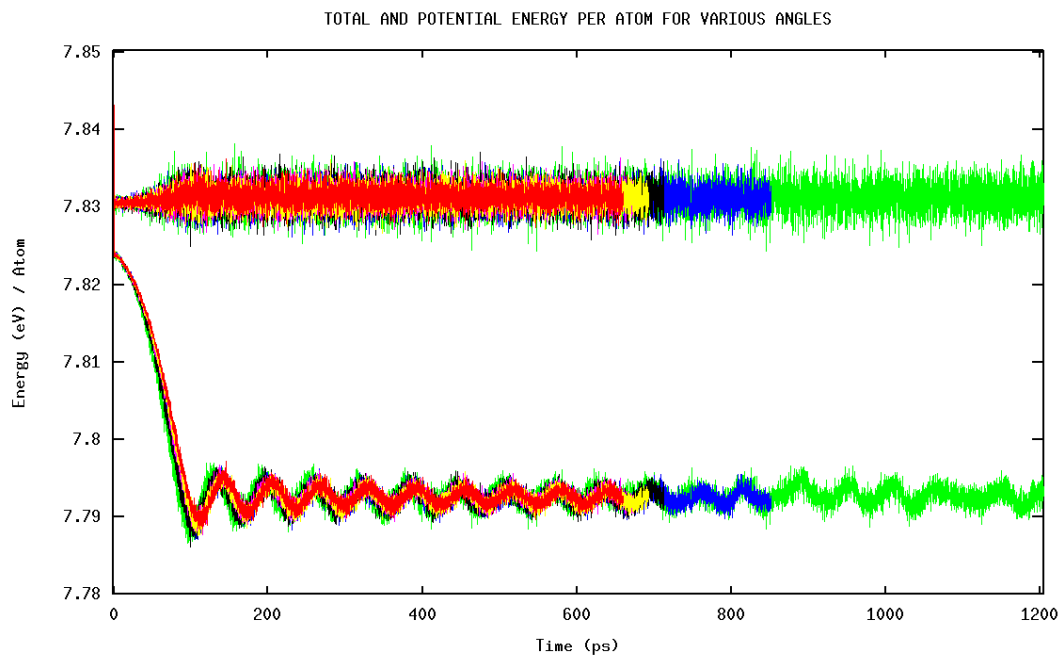


Figure 3.13: Total energy (higher) and potential energy (lower) per atom at 300K

Figure 3.14 shows the total and potential energy graphs for 4 different periodic moire patterns that are obtained by assigning the initial input parameters to the layers separately. In the graph, the red line corresponds to a periodic double layer with 1256 atoms and a 7.92-degrees

twisting angle, the yellow line corresponds to 608 atoms and a 13.17-degree twisting angle, the green line corresponds to 248 atoms and a 17.90-degree twisting angle, and finally, the blue line corresponds to 104 atoms and a 27.90-degree twisting angle. The temperature fluctuates around 9K.

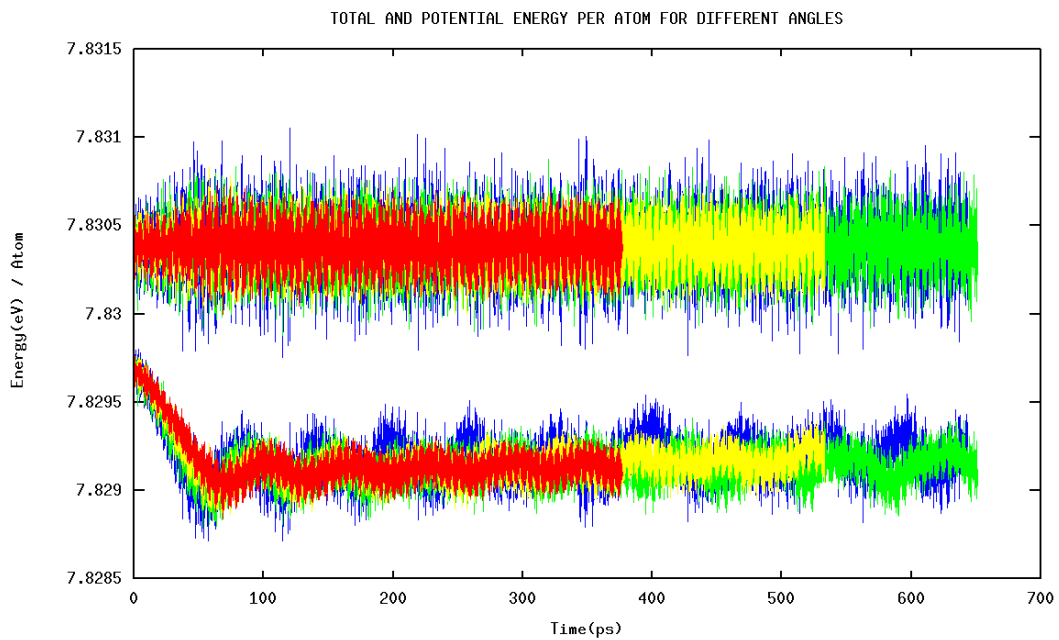


Figure 3.14: Total energy (higher) and potential energy (lower) per atom at 9K

The results of the experiment-2 show that the potential energy are same for different moire angles. Total energy is constant at 7.83eV per atom both at 300K and 9K. However at higher temperature potential energy is lower. The sliding of the layers with respect to each other has been reduced in the second experiment. It could not be eliminated completely for the cases with low number of atoms at small temperatures. Some special cases have also been observed: No sliding occurred in 4424-atoms simulations; however, this system was not thermally equilibrated. For a 1016-atoms system with a twisting angle of 13.17 at 300 K, sliding of the hexagonal pattern is observed, as shown in Figure 3.15. Figure 3.16 shows the energy of the system for the 1016-atom case.

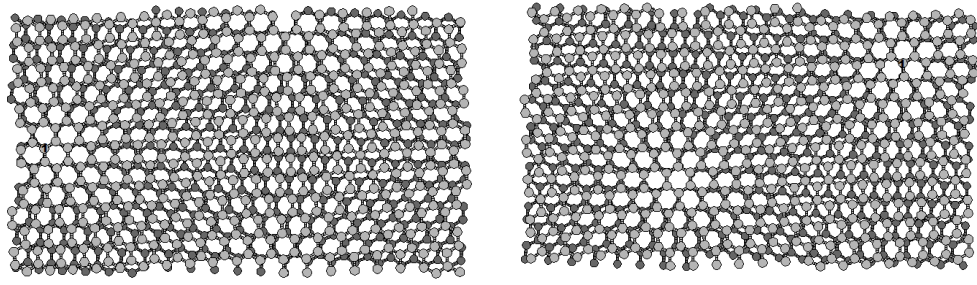


Figure 3.15: The image at the left side shows the moire pattern at 313 ps, and the image at the right side shows the moire pattern at 328 ps. Periodic graphene double layer includes 1016 atoms and a 13.17-degree twisting angle. The pattern moves in the direction of chiral path at 300K.

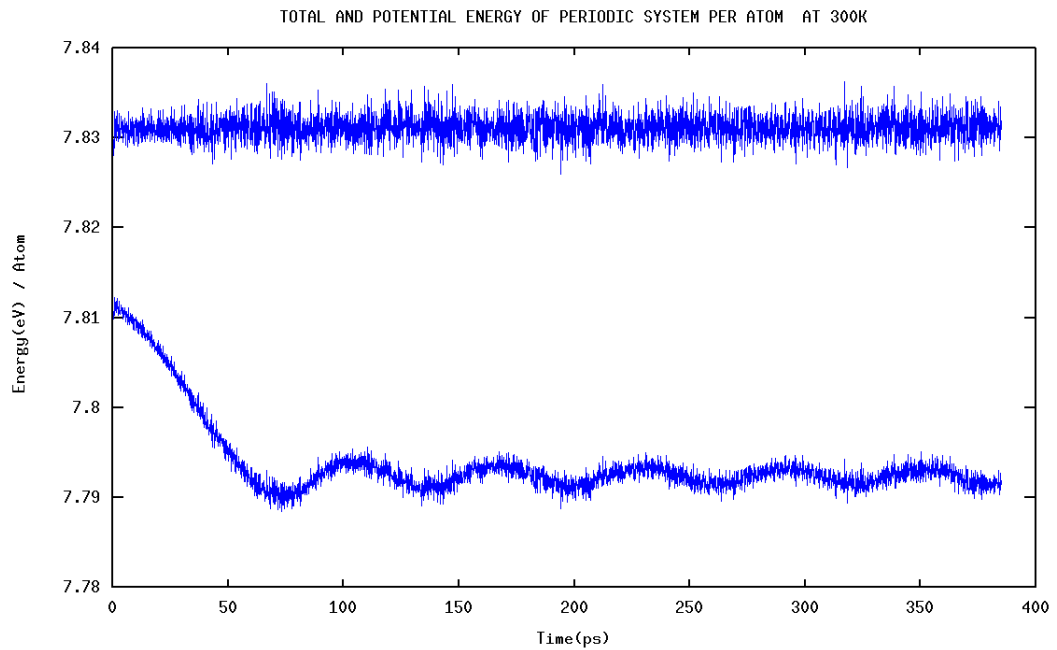


Figure 3.16: Total energy (higher) and potential energy (lower) per atom at 300K for the periodic system which has 1016 atom and twisting angle of 13.17 degrees

This experiment showed that the sliding of the layers is not caused by the defined initial conditions. In fact, the sliding process has been observed in recent computational studies as a property of few layer graphenes [52,53].

### **3.3 EXPERIMENT 3: Relaxed Graphene Identified According to Layers**

In this experiment atoms are grouped into four type. These are carbons of the first layer, carbons of the second layer, hydrogens of the first layer, hydrogens of the second layer. Velocity and thermostat information are assigned separately. Angular momentum equaled to zero for each 10 step. That prevents the rotation in the box. However, twisting of the layers are continued. This experiment is performed for double layer graphene flake which has 428 atoms at temperature of 10K. Initial angles starts from 6 degrees to 60 degrees. Not all these angles shows stability. The results which are more stable are shown.

#### **3.3.1 Graphene Flake With 428 Atoms at 10K**

Molecular dynamics simulations are performed for double layer graphene which have 428 atoms at 10K. Initial angles are taken from 6 degrees to 60 degrees. Sliding of layers on each other and movement of the flakes in the simulation box create problem for calculation of twisting angles. Because sliding is small at low temperature, twisting angle of layers with respect to each other can be calculated. Reference plane is taken as a plane which is perpendicular to axes passes through the central atoms. In the following, vectors from central atoms to neighbors are defined. The angle between projections of these vectors on defined plane gives twisting angle of one layer with respect to the other layer. The calculated results are given in graphs below. When initial angles are taken from 6 to 14 degrees the system stabilize at around 8.5 degrees as seen in the Fig.3.17. Initial twisting angles between 15 and 23 are given in the Figure 3.18. Pink colored line starts from 15 degrees and ends at 12.7 degrees while initial angles started at 16, 17, 18, 19 (blue,green,red,cyan lines) end at 15 degrees. Angle which is initially 20 degrees falls down to 8.5 degrees but initial angles starts from 21,22,23 degrees falls down to approximately 7 degrees. The other final angle, which most of simulations end at is 47.7 degrees. Initial angles taken from 42 to 51 degrees tend to go 47.7 degrees as shown in Fig.3.19. As naturally, the other stable twisting angle is 60 degrees. The initial angles started from 52 to 59 degrees rise to that value. This can be seen in Fig.3.20.

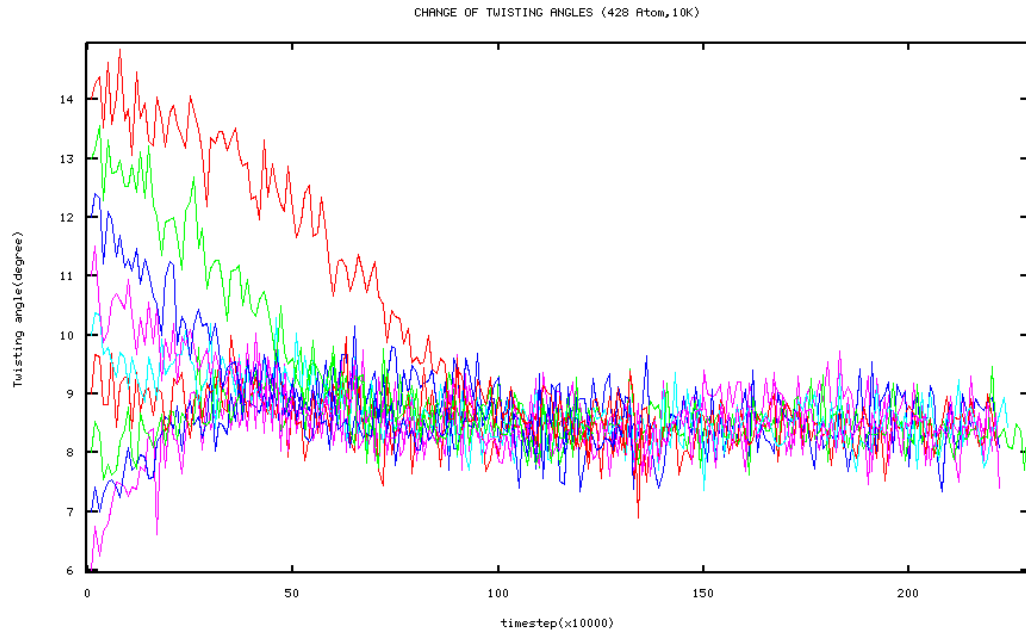


Figure 3.17: Graphene flake has 428 atoms at around 10K. Different twisting initial angles begin from 6 degrees to 14 degrees stabilize at around 8.5 degrees along 2,200,000 timestep.

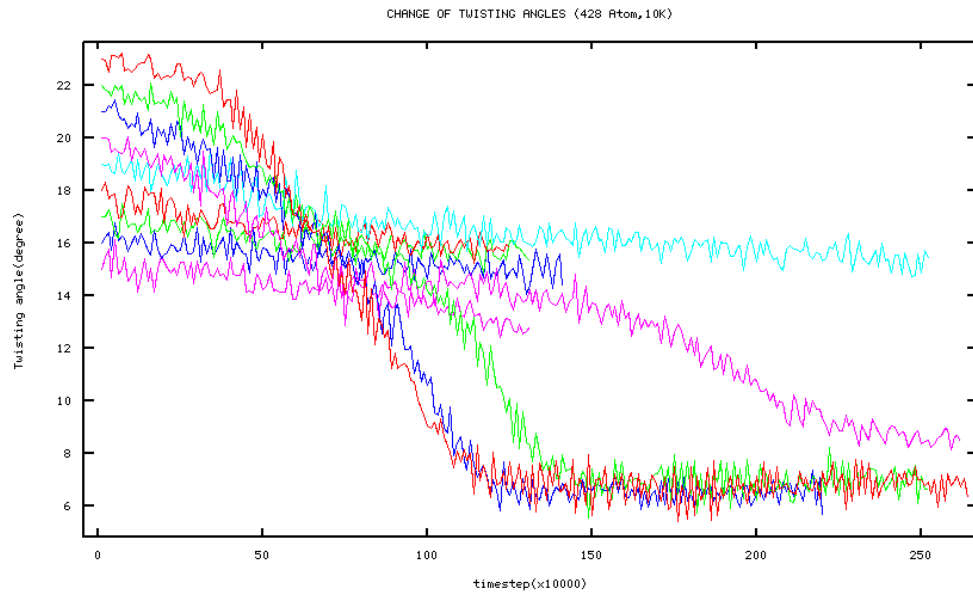


Figure 3.18: Graphene flake has 428 atoms at around 10K. Various initial twisting angles started from 15 to 23 degrees are shown. Initial angles starting from 21, 22, 23 degrees fall down to approximately 7 degrees.

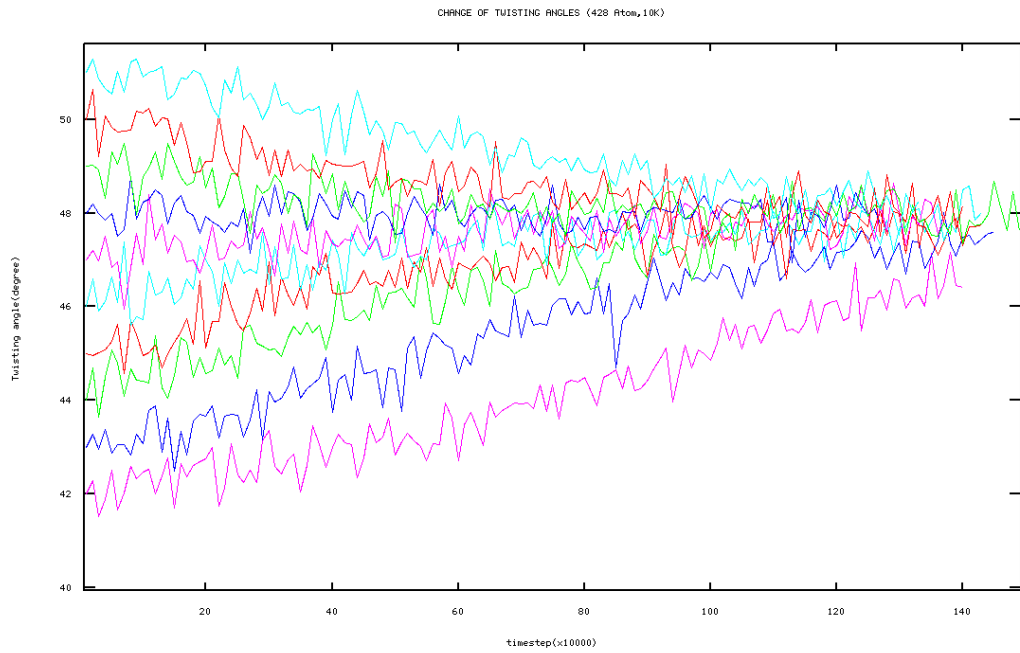


Figure 3.19: Graphene flake has 428 atoms at around 10K. Initial twisting angles started from 42 degrees to 51 degrees takes the approximate value of 47.7 degrees.

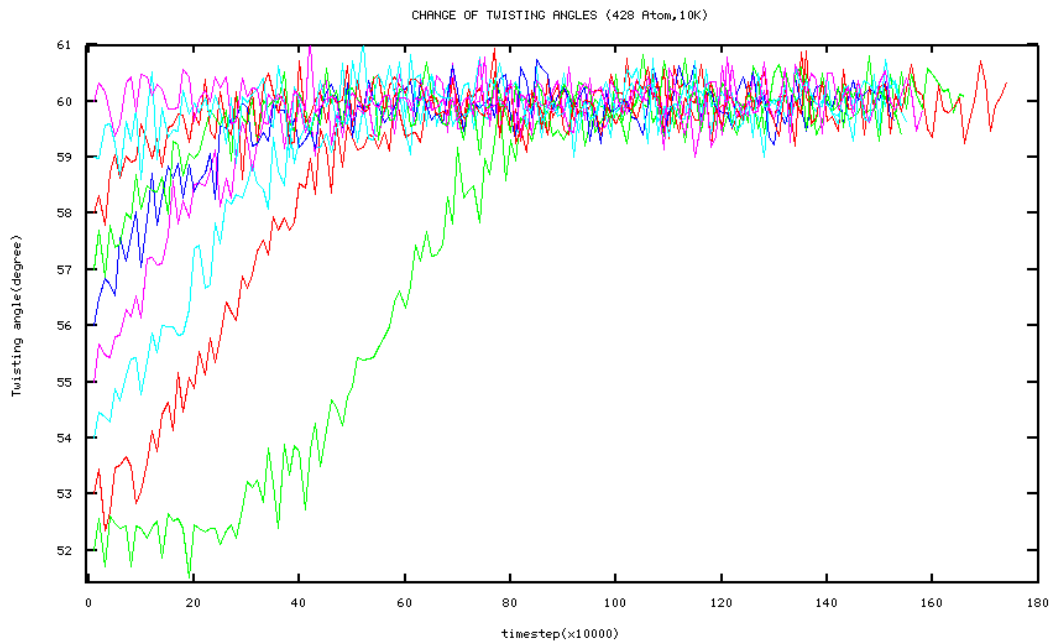


Figure 3.20: Graphene flake has 428 atoms at around 10K. Initial twisting angles started from 52 degrees to 60 degrees take average final value of 60 degrees.

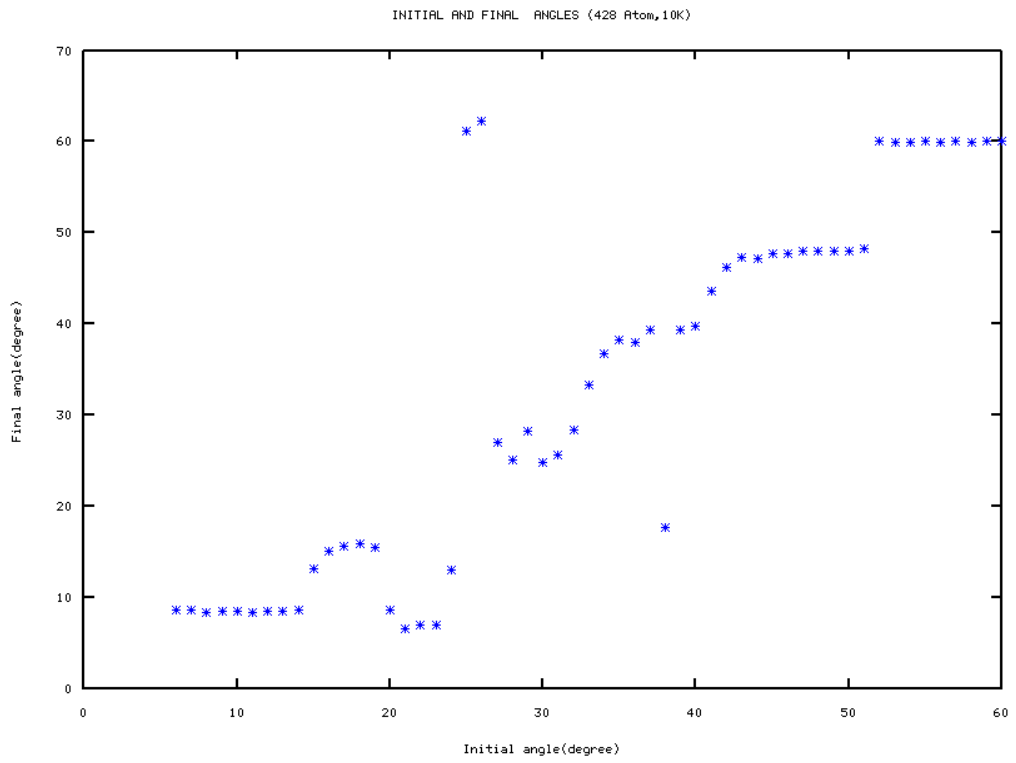


Figure 3.21: Graphene flake has 428 atoms at around 10K. Initial twisting angles started from 6 degrees to 60 degrees and corresponding final angles are shown. Final angles of 60, 47.7 and 8.5 shows most stable conditions.

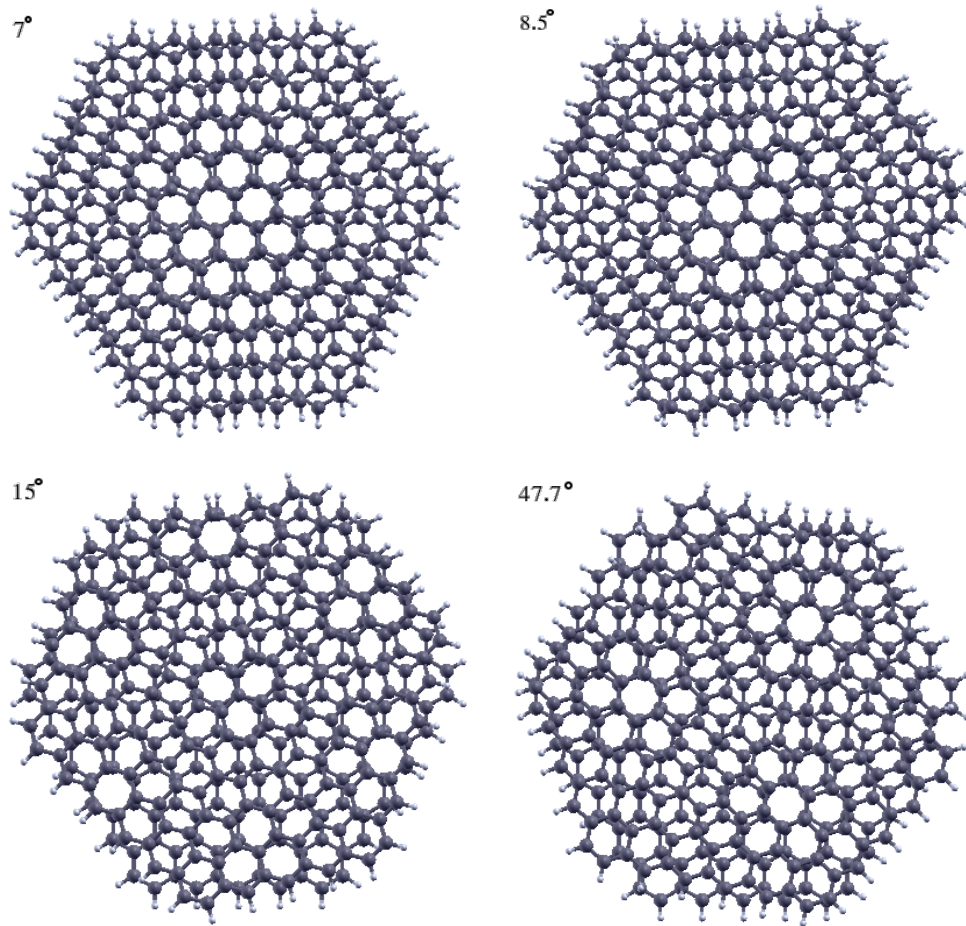


Figure 3.22: The images of graphene flakes with 428Å.

### 3.4 EXPERIMENT 4: Stretched Graphene

Changing of the moiré patterns and rotation of the graphene flakes within the simulation box were needed to be eliminated. Consequently, the hydrogen atoms around the flake are not identified as individual atoms, instead, they are identified as rigid bodies in the LAMMPS input code. However, the rotation in the simulation box persisted, and the potential energy kept fluctuating in a wider energy range. Furthermore, some of the flakes are splintered due to stress especially at high temperature. At low temperature (10K) some of C-C bonds near the edge are broken however, flakes do not splinter (Fig.3.23 and 3.24). Sliding of layers prevented thus, potential energy with respect to twisting angle show variation. This can be seen from Fig.3.25

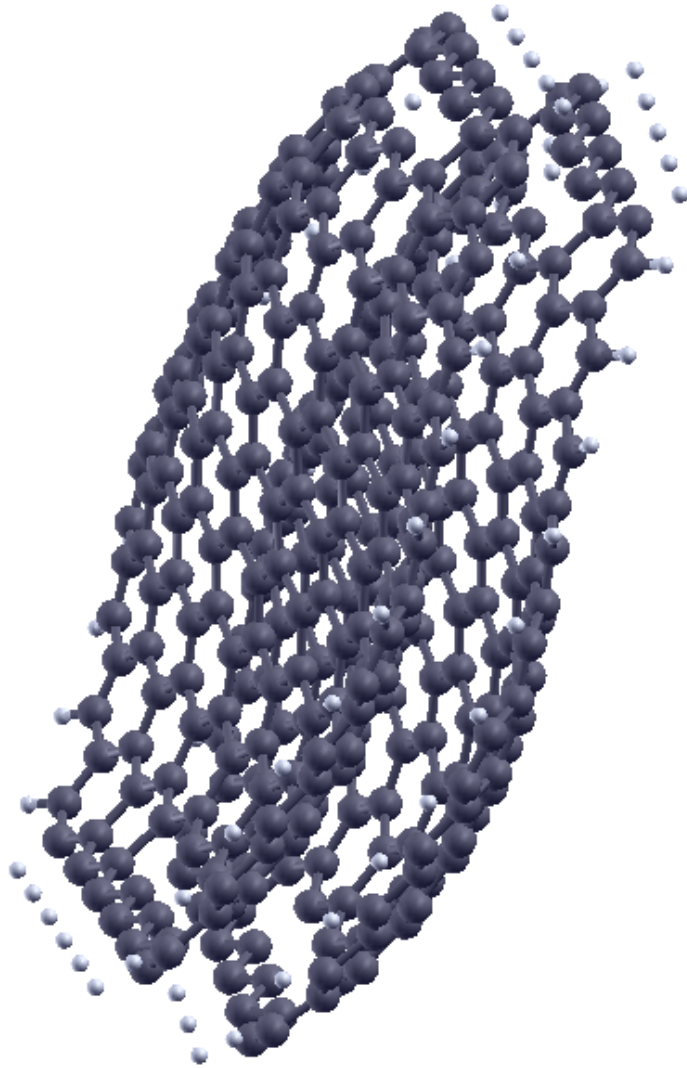


Figure 3.23: Perspective view of graphene flake which has 428 atoms at around 10K at the timestep of 821.000. Some bonds near edge are broken because of stress. Initial angle is given as 5 degrees

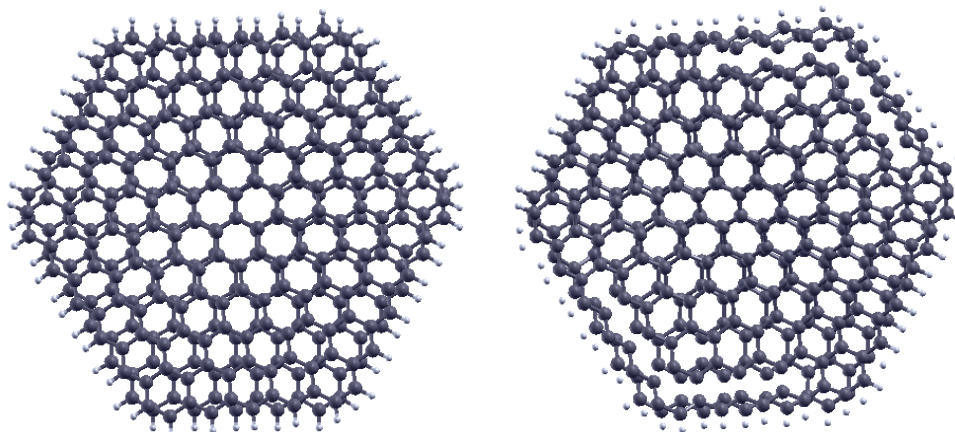


Figure 3.24: Initial and final view of graphene flake which has 428 atoms at around 10K. Some bonds near edge are broken because of stress. Initial angle is given as 5 degrees

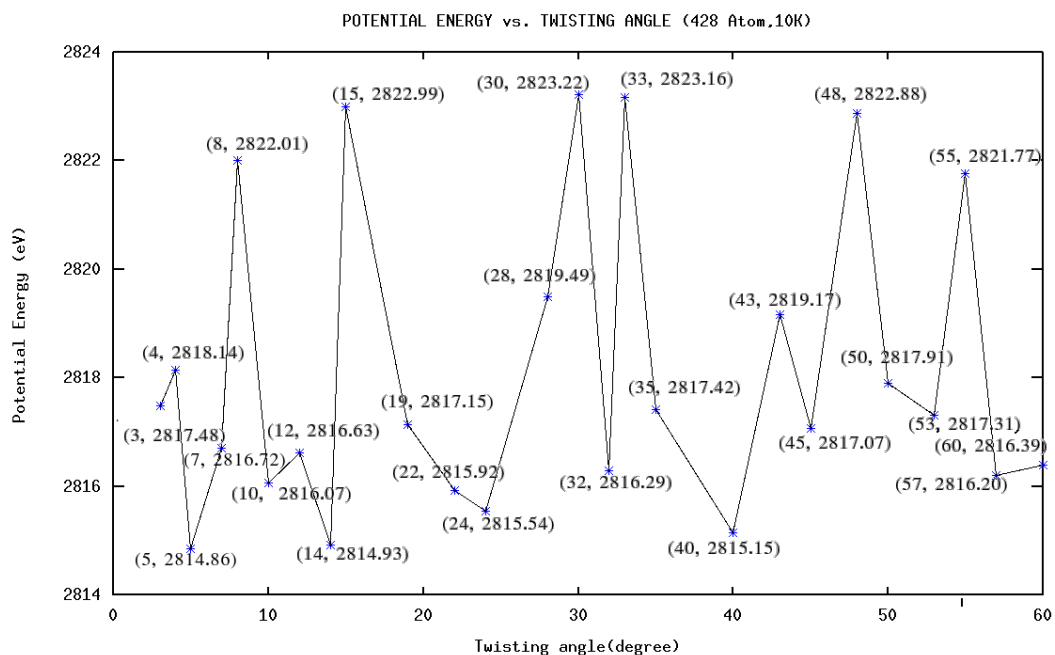


Figure 3.25: Average potential energy at with given initial theta of graphene flakes which has 428 atoms at 10K. Potential wells are seen between maximum points. First maximum occurs at 8 degrees with the potential energy 2822.01 eV; Second maximum occurs at 15 degrees with 2822.99 eV; Third maximum occurs at 30 degrees with 2823.22 eV; Forth maximum occurs at 33 degrees with the potential energy of 2823.16eV; Fifth maximum is at 48 degrees with 2822.88 eV and last maximum is at 55 degrees with 2821.77 eV.

## CHAPTER 4

### CONCLUSION

Before the discovery of graphene Moire patterns, graphene was assumed to be found in rhombohedral form in the nature. When graphene was successfully stabilized by Andre Geim and Konstantin Novoselov, the studies on graphene gained momentum. Moire patterns were observed by scanning tunnelling microscopy (STM) and high resolution transmission electron microscopy (HR-TEM). However, the stability of these structures is still largely uncharted. For this purpose, this thesis addresses this subject, and for the first time in the literature, it investigates the molecular dynamics of moire patterns observed in graphene double layers using LAMMPS (Large-scale Atomic/Molecular Massively Parallel Simulator), which is a software with a GNU general public license.

The first step to observe moire patterns is to create them. This is achieved in our study by home-written Octave code. For simplicity of observing moire patterns, graphene double layers are created in hexagonal layers by constructing a shell model which is explained in chapter 2. Graphene flakes are terminated by hydrogen atoms to provide the  $sp^3$  bonding of the edge atoms of the flakes. These flakes are then twisted around an axis which is perpendicular to the layers and passing through the center of mass of flakes; thus, moire patterns are observed. In the next step, the periodicity condition for Moire patterns in the double layer graphene is derived by selecting the symmetry lines. In this thesis, various molecular dynamics simulations, referred to as 'experiments' in the thesis, are designed and performed in LAMMPS. 4 types of experiments designed in this study for the double layer graphene can be summarized as follows:

In the experiment-1, the initial parameters, such as the velocity distribution, are defined commonly for all layers. There are no grouped atoms except hydrogen and carbon atoms unlike

experiment4. Experiment-1 is performed at 0K with 3 different sized flakes. The first simulation of experiment-1 includes 1448 atoms, which corresponds to an N value of 10 in the derived shell model. Three different initial twisting angles are assigned for the first three simulations. The results of these simulations showed that the twisting angle stabilizes at 4.29 degrees, regardless of the initial angle. Then, a fourth simulation is performed with double layer flakes, which have 3884 atoms. In this simulation, graphene twisting angle falls down rapidly to 5 degrees, and after 8,000,000 steps (800ps), it falls down to 2.59 degrees. This pattern shows that there are transient phases in this case. In the fifth simulation of this experiment, the number of atoms is increased to 5288. Twisting angle of layers becomes stable at 4.53 degrees after 7,000,000 time step (700ps) in this final simulation of the experiment.

Experiment-2 is performed under periodic boundary conditions and represents infinitely large graphene layers at 10K. Two different kinds of simulations are performed in this experiment: In the first type, periodic moire patterns slide in the simulation box since the layers slid over each other, although the initial velocities are defined in a Gaussian distribution, which should have provided that the average velocity is zero. In order to solve this problem, the LAMMPS input is defined such that initial velocities with a Gaussian distribution are assigned to each layer separately in the second type. However, sliding of layers observed again. According to the this experiment there is no any potential energy change observed with respect to change of twisting angle. According to some references distance between AA stacking is larger than AB stacking graphite [54]. On the contrary of this, there is no specific change attributed to the stacking type is observed. This may be because of taking the lennard-jones cut off smaller. Any regulation according to distances between layers, which ranges from 3.30 to 3.48 is not found.

Experiment-3 is a different version of experiment-1 performed at a higher temperature (10K) and with graphene flake including 428 atoms. Different initial angles, from 6 to 60 degrees, are assigned to the graphene flakes. However, the twisting angle stabilized for only some of these initial angles: It settles at 8.5 degrees for the initial angles from 6 to 14 degrees, at 7 degrees for the initial angles of 21, 22, and 23 degrees, at 47.7 degrees for the initial angles between 43 and 51 degrees, and at 60 degrees as expected for the initial angles from 51 to 60 degrees.

In the experiments up to this point, sliding is observed in the layers, and there seems to be no

relation between the potential energy and the moire pattern. Therefore, a fourth experiment is performed. In experiment-4, sliding and turning of the layers with respect to each other are prevented by stretching the flakes to a rigid body. That is, the atoms around the flakes are modeled as a rigid body and construct some stress on the graphene flakes. According to this model potential wells are found. However behaviour of the experiment 3 can not be explained completely according to this results.

Bernal (AB) stacking is assumed to be in ground state whereas AA stacking is less preferred condition. Moire patterns include both of stacking types. In this study, the angle becomes stable in higher potential energy states this shows these are metastable states. This is mostly observed in the flakes with higher sizes. As the size of the flake is increased and the angle, defined according to AA stacking is at 0 degree, gets smaller to equilibrate the AA stacking and AB stacking percentage of areas. This study shows these geometric properties by molecular dynamics simulations. Therefore this simulations can lead to other studies in terms of choosing twisting angle. On the otherhand, observations of moire pattern on graphite is performed mostly with STM. In the experimental physics these graphene layers are mostly on a substrate. Therefore effect of substrate is also important. More information can be gathered by adding substrate into molecular dynamics simulation in the future works.

## REFERENCES

- [1] J.A.Elliott,"Novel approaches to multiscale modelling in materials science,"*International Materials Reviews*, Vol. 56, No. 4, 2011
- [2] Yasuaki Hiwatari,Yutaka Kaneko,Hiroaki Ishida "Molecular Simulation for Nanotechnologies: Application to Industry", *Molecular Simulation*, Vol.30 (13-15), pg. 819-826, 15 November-30 December 2004
- [3] J.M: Haile, "Molecular Dynamics Simulation," Ch1.6,pg18,A Willey Interscience Publication, Canada-1992
- [4] Nicholas J. Giordano,"Computational Physics", Chapter 9, Prentice Hall, 1997
- [5] B.J. Alder,T.E. Wainwright,"Phase Transition for a Hard Sphere System", *J. Chem. Phys.*, 27,p1208-1209, 1957
- [6] Loup Verlet,"Computer Experiments on Classical Fluids. I. Thermodynamical Properties of Lennard Jones Molecules",*Physical Review*, Vol.159, No.1, 5 July 1967
- [7] J.M: Haile, "Molecular Dynamics Simulation," Ch1.6.2,pg 17,A Willey Interscience Publication,Canada-1992
- [8] G.Ali Mansoori,"Principles Of Nanotechnology: Molecular Based Study Of Condensed Mater In Small Systems" Chapter 5, pg 147-148, World Scientific Pub. Co. Inc., 2005
- [9] J.S. Hansen ,J.T.Ottesen, "Molecular dynamics simulation of oscillatory flows in micro fluidic channels", *Microfluid Nanofluid*, 2, 301-307, 2006
- [10] Y.Zhang, H.Huang, "Do Twin Boundaries Always Strengthen Metal Nanowires?", *Nanoscale Res Lett*,4,34-28,2009
- [11] J.M: Haile, "Molecular Dynamics Simulation", Ch1.6.2, pg 18, A Willey Interscience Publication, Canada-1992
- [12] G.Ali Mansoori, "Principles Of Nanotechnology: Molecular Based Study Of Condensed Mater In Small Systems", Chapter 2, pg 38, World Scientific Pub. Co. Inc., 2005
- [13] J.E. Jones, "On the Determination of Molecular Fields. I. From the Variation of the Viscosity of a Gas with Temperature", *Proceedings of the Royal Society of London, Series A, Containing Papers of a Mathematical and Physical Character*, Vol. 106, No. 738, pp. 441-462, (Oct. 1, 1924)
- [14] Steve Plimpton, "Fast Parallel Algorithms for Short Range Molecular Dynamics", *Journal of Computational Physics*, Vol. 117, pg. 1-19, (1 March 1995)- originally Sandia Technical Report SAND91-1144 (May 1993, June 1994)
- [15] N.Zabararas, "Cornell University MEA715-Atomistic Modeling Of Materials Lecture Notes", 2010

- [16] J.M: Haile, "Molecular Dynamics Simulation," Ch4.4,pg 157-160, A Willey Inter-science Publication, Canada-1992
- [17] C.W.Gear, "The numerical integration of ordinary differential equations of various orders", Technical Report ANL 7126, Argonne National Laboratory, 1966
- [18] C.W.Gear, "Numerical Initial Value Problems In Ordinary Differential Equations", Prentice-Hall, Englewood Cliffs, NJ, 1971
- [19] C.A.Fuzo, L.Degrve "Effect of the thermostat in the molecular dynamics simulation on the folding of the model protein chignolin" J Mol Model,Vol 18, pp.2785-2794,2012
- [20] R.J. Sadus, "Molecular Simulation Of Fluids:Theory, algorithms and object orientation", Ch.8, Elsevier 2002
- [21] M.Cerioti et al., "Efficient stochastic thermostating of path integral molecular dynamics", Journal of Chemical Physics, 133, 124104-124104-13, (2010)
- [22] T.Soddemann et al., "Dissipative particle dynamics: A useful thermostat for equilibrium and nonequilibrium molecular dynamics simulations", Physical Review E, 68, 046702, 2003
- [23] C.Pastorino et al., "Comparison of Dissipative Particle Dynamics and Langevin thermostats for out-of-equilibrium simulations of polymeric systems", Physical Review E, 76, 026706, 2007
- [24] H.C. Andersen., "Molecular dynamics at constant pressure and/or temperature", J.Chem.Phys., 72, 2384-2393, 1980
- [25] D.Frenkel, B.Smit, "Understanding molecular simulation from algorithms to applications", Academic Press, 2002
- [26] C.P. Lowe, "An alternative approach to dissipative particle dynamics", Europhys. Lett., 47, 145, 1999
- [27] S.Nose, "A molecular dynamics method for simulations in the canonical ensemble", Molecular Physics, Vol 52, No. 2, pg. 255-268, 1984
- [28] Sukang Bae et all, "Roll-to-roll production of 30-inch graphene films for transparent electrodes", Nature Nanotechnology, Vol. 5, August 2010
- [29] Lucas H. Hess et all, "Graphene Transistor Arrays for Recording Action Potentials from Electrogenic Cells", Advanced Materials, 23, 5045-5049, 2011
- [30] Khan M. F. Shahil, Alexander A. Baladin, "Graphene-Based Thermal Interface Materials", 2011 11th IEEE International Conference on Nanotechnology,Portland Marriott, August 15-18, 2011, Portland, Oregon,USA
- [31] B.Partoens, F.M. Peeters, "From graphene to graphite:Electronic structure around the K point", Physical Review B 74, 075404, 2006
- [32] R.Saito,G.Dresselhaus,M.S.G.Dresselhaus,"Physical Properties Of Carbon Nanotubes", Imperial College Press 1998
- [33] A.C Neto, F.Guinea, N.M.Peres, "Drawing Conclusions From Graphene", Physics World, November 2006

- [34] S.H.Jhang et al., "Stacking-order dependent transport properties of trilayer graphene", *Physical Review B* 84, 161408(R), 2011
- [35] Tymofiy Khodkov et al., "Electrical transport in suspended and double gated trilayer graphene", *Applied Physics Letters* 100, 013114, 2012
- [36] A. H. Castro Neto et al., "The electronic properties of graphene", *Reviews Of Modern Physics*, Vol. 81, January-March 2009
- [37] M.F. Craciun et al., "Tuneable electronic properties in graphene", *Nano Today*, Vol. 6, pg. 42-60,2011
- [38] M.F. Craciun et al., "Massless fermions in multilayer graphitic systems with misoriented layers: Ab initio calculations and experimental fingerprints", *Physical Review B*, 76, 201402 (R), 2007
- [39] A.Luican et al., "Single-Layer Behavior and Its Breakdown in Twisted Graphene Layers", *Physical Review Letters*, PRL 106, 126802, 2011
- [40] E. Y. Andrei et al., "Electronic properties of graphene: a perspective from scanning tunnelling microscopy and magnetotransport", *Rep. Prog. Phys.*, 75, 056501 (47pp), 2012 IOP publishing
- [41] Isaac Amidror, "The theory of moire phenomenon", Volume 1: Periodic Layers, Second Edition, Springer, 2000
- [42] A.J.Durelli,V.J.Parks "Moire Analysis Of Strain" Prentice-Hall Inc, Englewood cliffs, N.J., 1970
- [43] H.S. Wong and C.Durkan, "Unraveling the rotational disorder of graphene layers in graphite", *Physical Review B*, 81, 045403, 2010
- [44] J. Xhie et al., "Giant and supergiant lattices on graphite", *Physical Review B*, Vol.47, No.3, 15 June 1993
- [45] D.L. Miller et al., "Structural analysis of multilayer graphene via atomic moire interferometry", *Physical Review B*, 81, 125427, 2010
- [46] F. Varchon et al., "Rotational disorder in few-layer graphene films on 6H-SiC(000-1): A scanning tunneling microscopy study", *Physical Review B*, 77, 165415, 2008
- [47] Manoj K. Singh, "Atomic scale observation of rotational misorientation in suspended few layer graphene sheets", *Nanoscale*, 2, 700-70, 2010
- [48] J.M. Campanera et al. "Density functional calculations on the intricacies of Moire patterns on graphite", *Physical Review B* 75, 235449, 2007
- [49] S.J.Stuart, A.B.Tutein, J.A.Harrison, "A reactive potential for hydrocarbons with intermolecular interactions", *J.Chem.Phys.*, Vol. 112, No. 14, April 2000
- [50] D.W. Brenner "Empirical potential for hydrocarbons for use in simulating the chemical vapor deposition of diamond films", *Physical Review B* 42, 9458-9471 (1990)
- [51] J. Tersoff, "New empirical approach for the structure and energy of covalent systems", *Phys.Rev.B* 37, 6991-7000, 1998

- [52] Oded Hod, "Interlayer commensurability and superlubricity in rigid layered materials", *Physical Review B* 86, 2012
- [53] Liang Xu et al., "Molecular dynamics simulation of the interlayer sliding behavior in few-layer graphene", *Carbon*, 50, 1025-1032, 2012
- [54] J. Berashevich, T. Chakraborty "On the Nature of Interlayer Interactions in a System of Two Graphene Fragments", *J. Phys. Chem. C*, 115, 24666-24673, 2011